Podoplanin function is switched by partner proteins on fibroblastic reticular cells

Charlotte M. de Winde[1], Spyridon Makris[1,*], Lindsey Millward[1,*], Agnesska C. Benjamin[1], Giulia Cazzagon[1], Victor G. Martinez[1], and Sophie E. Acton[1,✉]

[1]Stromal Immunology Group, MRC Laboratory for Molecular Cell Biology, University College London, Gower Street, London, WC1E 6BT, United Kingdom
[*]These authors contributed equally

Podoplanin is an inflammatory marker upregulated in many pathologies and correlated with invasive cell behaviour. Podoplanin is reported to facilitate both actomyosin contractility and formation of cell protrusions. However, how podoplanin can elicit these opposing phenotypes is unknown. We examined podoplanin functions in lymph node fibroblastic reticular cells (FRCs), with high endogenous podoplanin expression. We report that podoplanin expression, localisation and function are dependent on partner proteins. CLEC-2 binding upregulates podoplanin transcription, and tetraspanin CD82 is essential for trafficking of podoplanin to the plasma membrane. At the cell surface, podoplanin regulates cytoskeletal dynamics, balanced by its membrane binding partners hyaluronan receptor CD44 and tetraspanin CD9. Both CD44 and CD9 dampen podoplanin-dependent actomyosin contractility, and *in vitro*, CD9/podoplanin promotes filopodia-like protrusions whereas CD44/podoplanin promotes lamellipodia formation. Both CD44 and CD9 are required to coordinate protrusion formation and spreading of FRCs in response to CLEC-2^{+} dendritic cells, a requirement for acute lymph node expansion. *In vivo*, surface expression levels of podoplanin, CD44 and CD9 are specifically upregulated on T-cell zone FRCs in the early phase of lymph node expansion. Our data support a model whereby podoplanin resides in distinct plasma membrane domains, and that CLEC-2 binding serves as a molecular switch to change podoplanin function.

Podoplanin | CD44 | CD9 | CD82 | Tetraspanins | Fibroblastic reticular cell | Lymph node

Correspondence: ***s.acton@ucl.ac.uk***

Introduction

Podoplanin was discovered almost simultaneously in a wide variety of tissues and cell types, and has therefore been assigned multiple names (podoplanin, gp38, Aggrus, PA2.26, D2-40, T1α) based on its function in different contexts (1). This type I transmembrane mucin-like glycoprotein is expressed on the surface of kidney podocytes, osteocytes, glial cells, type I alveolar cells, skin keratinocytes, lymphatic endothelial cells (LECs), and some fibroblast subsets (2–9). Podoplanin plays a pivotal role in the correct development of heart, lungs, secondary lymphoid tissues and lymphatic vasculature. Podoplanin *null* mice exhibit embryonic lethality due to cardiovascular problems or die shortly after birth of respiratory failure (10–12), and exhibit defective blood-lymphatic vasculature separation (13, 14), so understanding the full range of podoplanin functions in other tissues has been challenging.

Podoplanin expression levels are dynamic through development and in pathological conditions. Upon wounding, epidermal keratinocytes increase podoplanin expression (15), and in sepsis, inflammatory macrophages express podoplanin (16). In many types of cancer, podoplanin is upregulated both on tumour cells and on cancer-associated fibroblasts (CAFs) in the tumour microenvironment (1, 17). In homeostasis, lymph nodes express high levels of endogenous podoplanin (7), which increases upon *in vivo* immunization (18). Interestingly, follicular lymphoma-bearing lymph nodes show decreased podoplanin expression (19). The molecular mechanisms controlling these changes in podoplanin expression are not fully understood. In skin, brain and bone tumour cells, the podoplanin gene *Pdpn* is under control of the transcription factor activator protein 1 (AP-1) (20–22), but in LECs, *Pdpn* is expressed under the control of *Prox1* (23). It is therefore likely that podoplanin expression can be regulated by multiple signalling pathways depending on cell type, tissue context and inflammatory cues.

Podoplanin activity is involved in many different cell phenotypes and functions. In fibroblastic reticular cells (FRCs), podoplanin drives actomyosin contractility and controls cell stiffness through ERM binding (24, 25). Upon initiation of an immune response, CLEC-2^{hi} migratory dendritic cells bind podoplanin on FRCs inhibiting actomyosin contractility, resulting in FRC spreading and elongation for rapid lymph node expansion (24, 25). Furthermore, podoplanin expression by FRCs is essential for lymph node development, and FRC function can also be altered by binding of CLEC-2-expressing platelets (26, 27). In LECs, podoplanin binding to galectin-8 supports adhesion to the extracellular matrix (28), whereas in epidermal keratinocytes, podoplanin expression is inversely correlated with β1 integrin-mediated adhesion (29). Further studies have focused on the role of podoplanin in cell motility. In mesenchymal stromal cells, it has been shown that podoplanin expression is required for Rac1-dependent migration (30). Furthermore, podoplanin drives cell migration of CAFs (31) and cancer cells (32, 33), and as such plays a role in several stages of the metastasis process (1). Podoplanin is expressed at the invasive front of tumours (34), and more specifically recruited to the adhesion ring of invadopodia where it localizes in lipid rafts (35). In addition, podoplanin-dependent regulation of ezrin and moesin activates RhoA, driving epithelial-to-mesenchymal transition (36). We ask what molecular mechanisms permit one mem-

brane protein to drive these varied and sometimes contradictory phenotypes.

Since podoplanin has a very short cytoplasmic tail consisting of only nine amino acids (37), it is suggested that podoplanin would require binding partners to execute its diverse range of functions. Many binding partners have already been identified (1, 17), but their functions have mainly been described in the context of podoplanin upregulation in cancer. In this study, we seek to understand the function of endogenous podoplanin-binding partner interactions on FRCs in the normal physiology of immune responses.

Tetraspanins and interacting membrane proteins can link extracellular cues to intracellular signalling. Tetraspanins are a superfamily of four-transmembrane proteins that form tetraspanin-enriched microdomains via interactions with each other and binding partners. These microdomains spatially organize the plasma membrane into a tetraspanin web, which facilitates cellular communication (38, 39). We studied the role of two known podoplanin membrane binding partners in regulating FRC function: the hyaluronan receptor CD44 (33) and tetraspanin CD9 (40). The interaction of podoplanin with CD9 is mediated by CD9 transmembrane domains 1 and 2, and this interaction impairs cancer metastasis by inhibiting platelet aggregation (40). In contrast, the podoplanin/CD44 interaction at tumour cell protrusions promotes cancer cell migration (33). In NIH/3T3 fibroblasts, co-expression of CD44 and podoplanin reversed the hypercontractile phenotype seen in cells overexpressing podoplanin (24), suggesting an inhibitory function for CD44 in driving actomyosin contractility in fibroblasts. It has previously been shown that podoplanin and CD44 both reside in lipid rafts on MDCK cells (41). CLEC-2 binding to FRCs drives podoplanin clustering into cholesterol-rich domains (24), but the function of these podoplanin clusters is unknown. Another protein potentially involved in podoplanin-driven actomyosin contractility is tetraspanin CD82, since osteoclasts lacking CD82 expression show disrupted actin structures due to defects in RhoGTPase signalling, and a dramatic decrease in podoplanin expression (42). In prostate cancer cells, CD82 expression controls RhoGTPase activity and lamellipodia protrusions (43).

Here, we report that podoplanin surface expression on FRCs is dependent on presence of tetraspanin CD82. Podoplanin membrane binding partners CD44 and CD9 both stabilise podoplanin surface levels, and temper FRC hypercontractility. Binding of CLEC-2 serves as a molecular switch to change podoplanin function, reducing actomyosin contractility, and inducing FRC spreading and protrusion formation. CD44 and CD9 both contribute to FRC spreading by balancing lamellipodia and filopodia-like cell protrusions, respectively. Furthermore, during early phases of lymph node expansion when FRC spreading is observed (24, 25), both CD44 and CD9 are upregulated on T-cell zone FRCs.

Results

Tetraspanin CD82 is required for podoplanin membrane expression. Podoplanin drives actomyosin contractility in FRCs (24, 25). Tetraspanin CD82 also controls cytoskeletal structures via RhoGTPase signalling (42–45), and loss of CD82 in osteoclasts decreases the level of podoplanin expression (42). We hypothesized that tetraspanin CD82 may regulate podoplanin-driven actomyosin contractility in FRCs. We generated CD82 knock-out (KO) FRCs using CRISPR/Cas9 editing and selected single-cell clones by quantitative RT-PCR (Supplementary Fig. 1). Interestingly, CD82 KO FRCs almost completely lack podoplanin surface expression (Fig. 1a). To rule out an off-target effect of the CRISPR single guide RNA in the podoplanin gene (*Pdpn*), we generated CD82 KO clones in a podoplanin KO FRC cell line containing a doxycycline-inducible construct to re-express exogenous podoplanin (Supplementary Fig. 1). In support of our original observations, FRCs lacking CD82 are also unable to express exogenous podoplanin in this inducible system (Fig. 1b). Further, we transiently transfected control and CD82 KO FRCs with CFP-tagged podoplanin (PDPN-CFP; Fig. 1c). Flow cytometry reveals that CD82 KO FRCs lack surface expression of both endogenous and CFP-tagged podoplanin (Fig. 1c), but transfection efficiency and CFP expression is comparable to controls (Fig. 1d). Since the CFP signal is derived from the PDPN-CFP fusion protein, we conclude that PDPN-CFP is expressed by CD82 KO cells, but that tetraspanin CD82 controls intracellular protein trafficking of podoplanin to the plasma membrane, a well-known function of other tetraspanin family members (46). Conversely, *Cd82* expression is decreased in podoplanin shRNA knockdown (PDPN KD) FRCs, and CLEC-2 binding decreases *Cd82* expression (Supplementary Fig. 1). Together, these data indicate a co-regulation and interdependence between CD82 and podoplanin expression in FRCs.

CD44 and CD9 control podoplanin membrane expression and balance hypercontractility. Next, we sought to investigate the role of two known membrane binding partners of podoplanin in modulating its expression and function: the hyaluronan receptor CD44 (33) and tetraspanin CD9 (40). It has been shown that podoplanin-mediated hypercontractility can be counterbalanced by sufficient CD44 expression (24, 33), which requires podoplanin to re-localise to cholesterol-rich domains (24). Indeed, cholesterol depletion in FRCs results in hypercontractility and cell rounding in a podoplanin-dependent manner (24). Tetraspanins are predicted to have an intramembrane cholesterol binding pocket controlling their activity (47). We hypothesise that podoplanin activity in FRCs is balanced through changing microdomains in the plasma membrane, stabilised by membrane binding partners CD44 and CD9.

First, we investigated the membrane co-localisation of CD44 and CD9 with podoplanin on FRCs. CD44 is expressed over the whole cell membrane, but is enriched at the cell periphery where CD44 co-localises with podoplanin (Fig. 2a). In contrast, CD9 is present in punctate structures along the cell periphery and enriched in filopodia-like protrusions, where it partially co-localises with podoplanin (Fig. 2b). Neighbouring FRCs use $CD9^{+}$/$podoplanin^{+}$ filopodia-like protrusions to interact (Fig. 2b). These data indicate that CD44 and CD9

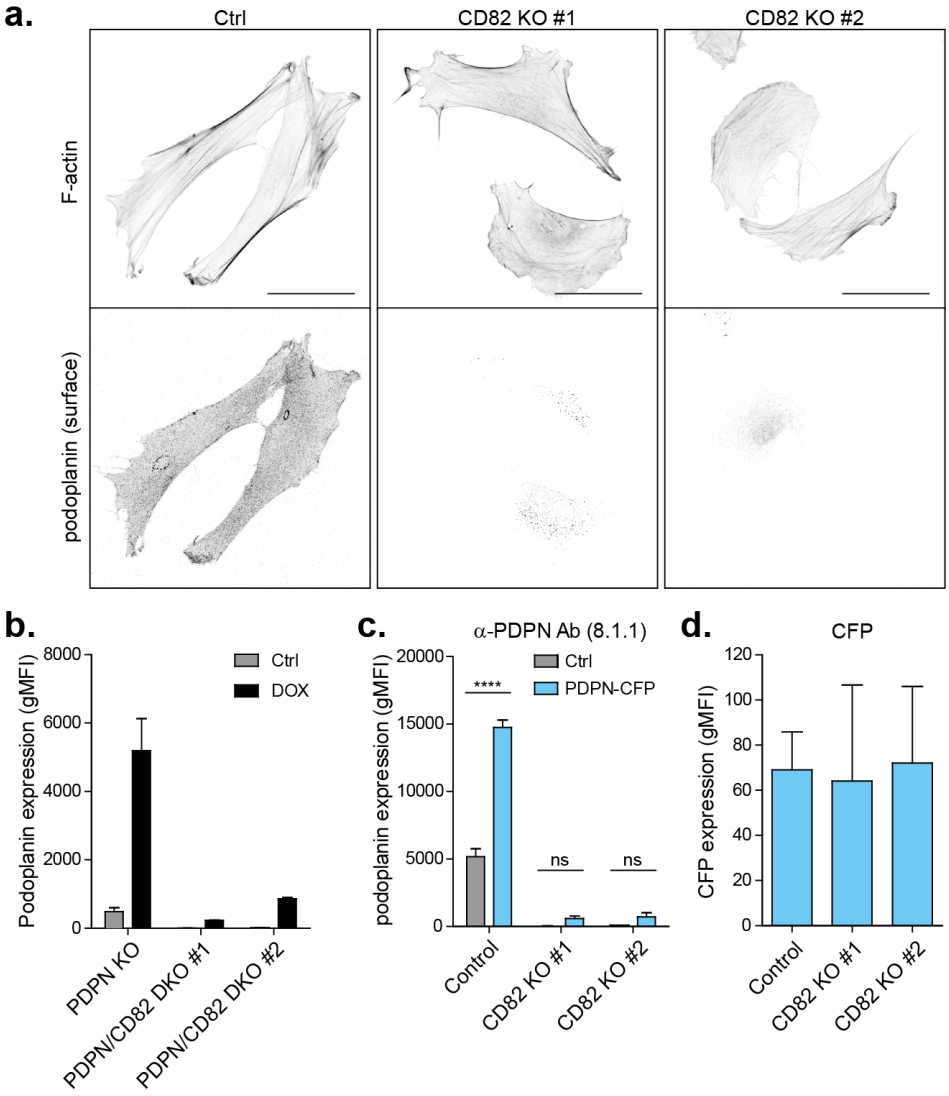

Fig. 1. Tetraspanin CD82 regulates podoplanin expression and localisation. **a.** Immunofluorescence of podoplanin surface expression (bottom row) on control (Ctrl) and two CD82 knock-out (KO) FRC cell lines. F-actin staining is used to visualise individual FRCs (top row). Maximum Z stack projections of representative images from n=3 biological replicates are shown. The scale bars represent 50 microns. **b.** Podoplanin KO (PDPN KO) and podoplanin/CD82 double-KO (PDPN/CD82 DKO) FRCs expressing a doxycycline-driven podoplanin-inducible plasmid were cultured in absence (grey) or presence (black) of doxycycline (DOX) for 48 hours. Podoplanin surface expression was analysed by antibody labelling using flow cytometry. **c-d.** Control (grey) and two CD82 KO FRC cell lines (blue) were transfected with CFP-tagged podoplanin (PDPN-CFP). Podoplanin surface expression using anti-mouse podoplanin antibody (clone 8.1.1; **c**) or CFP (**d**) expression was analysed by flow cytometry. **b-d.** Data shown as mean+SD collated from n=3 biological replicates. ****p<0.0001. ns, not significant. gMFI, geometric mean fluorescence intensity.

both co-localize with podoplanin. However, CD44 and CD9 reside in different subcellular locations, supporting a model of distinct pools of podoplanin on the FRC cell membrane, which may have different functions.

To differentiate the roles of CD44 and CD9 in these distinct podoplanin pools on the FRC plasma membrane, we generated CD44 KO, CD9 KO and CD44/CD9 double knockout (DKO) polyclonal FRC lines using CRISPR/Cas9 editing (Fig. 2c). Deletion of either CD44 or CD9 in FRCs results in approximately 25% reduction of podoplanin surface expression compared to control FRCs (Fig. 2c), suggesting that the availability of these binding partners impacts podoplanin expression levels at the plasma membrane.

The predominant phenotype of podoplanin over-expression is high actomyosin contractility (24). FRCs remain spread in the absence of either CD44 or CD9, and exhibit F-actin stress fibres similarly to control cells, indicating that the balance between contraction and spreading is maintained. However, simultaneous deletion of both CD44 and CD9 (CD44/CD9 DKO) markedly increases FRC contractility (Fig. 2d), despite podoplanin levels being lower than in control cells (Fig. 2c). CD44/CD9 DKO cells round up and exhibit membrane blebbing (approximately 40% of cells; Fig. 2d). To test whether the observed hypercontractility in CD44/CD9 DKO FRCs was podoplanin-dependent, we exposed cells to continuous CLEC-2-Fc, which inhibits podoplanin-driven actomyosin contractility (24, 25), and found that CLEC-2 CD44/CD9 DKO FRCs remained spread (Fig. 2d). These results suggest that both CD44 and CD9 inhibit podoplanin-driven contractility, but that in the absence of one binding partner, the other is able to dampen podoplanin-driven hypercontractility.

Podoplanin ligand function is independent of CD44 or CD9. Podoplanin can directly bind to CD44 and/or CD9 (33, 40), but it is unclear whether these complexes simply inhibit podoplanin-driven contractility, or actively contribute to other podoplanin functions. Podoplanin function on FRCs was first described as a ligand promoting both platelet aggregation and dendritic cell migration (14, 48). We tested

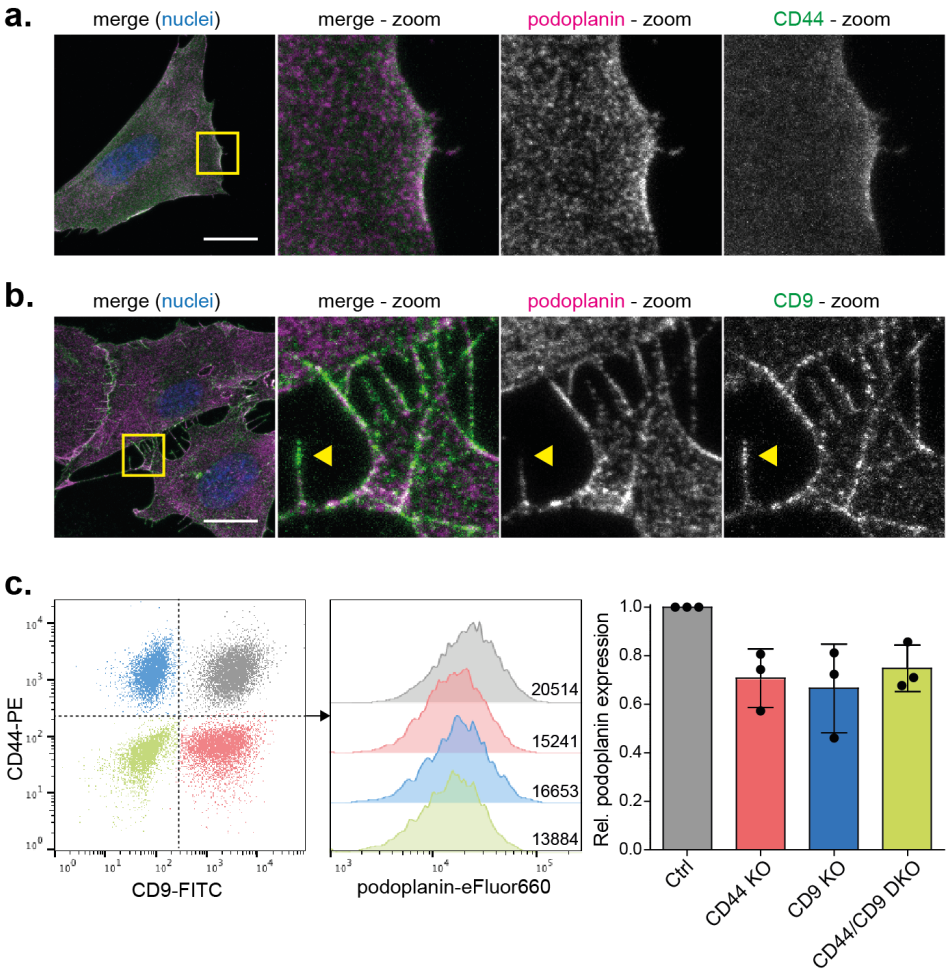

Fig. 2. CD44 and CD9 are required for stable podoplanin membrane expression and balancing hypercontractility. a-b. Immunofluorescence of podoplanin (magenta) and CD44 (**a**; green) or CD9 (**b**; green) in control FRCs. Maximum Z stack projections of representative images from n=3 biological replicates are shown. The scale bars represent 20 microns. Yellow arrow head indicates filopodia tip. **c.** Analysis of podoplanin surface expression on control (Ctrl; grey), CD44 knock-out (KO; red), CD9 KO (blue), and CD44/CD9 double-KO (DKO; green) FRC cell lines by flow cytometry. Podoplanin expression is normalized to the level in Ctrl FRCs for each individual experiment. Data shown as meanwith dots representing biological replicates (n=3). **d.** Left: Immunofluorescence of F-actin (black) and cell nuclei (blue) in Ctrl (grey), CD44 KO (red), CD9 KO (blue), CD44/CD9 DKO (green), and CLEC-2 CD44/CD9 DKO (white) FRC cell lines. Maximum Z stack projections of representative images are shown. The scale bars represent 50 microns. Right: Proportion of contracted FRCs. Data shown as meanwith dots representing n=11-15 images per cell line collated from 3-4 biological replicates. **p=0.0023, ***p=0.0009, ****p<0.0001. ns, not significant (p=0.0528).

whether CD44 or CD9 expression by FRCs is required for podoplanin ligand function using a three-dimensional co-culture of FRCs with bone marrow-derived CLEC-2$^+$ dendritic cells (49). Contact with podoplanin$^+$ FRCs induces dendritic cells to extend protrusions, in a CLEC-2 (48) and tetraspanin CD37-dependent manner (50). Whereas dendritic cells co-cultured with PDPN KD FRCs do not spread or make protrusions (Fig. 3a), co-culture of dendritic cells with CD44 KO or CD9 KO FRCs does not hamper dendritic cell responses (Fig. 3a). Furthermore, the increase in morphology index (=perimeter^2/4πarea) is equivalent to dendritic cells co-cultured with control FRCs (Fig. 3b). Therefore, podoplanin ligand function is not dependent on CD44 or CD9 expression on FRCs. This is in agreement with published data showing that soluble recombinant podoplanin-Fc can induce dendritic cell protrusions (48, 50).

CD44 and CD9 control FRC spreading in response to CLEC-2$^+$ dendritic cells. Since neither CD44 or CD9 are required for podoplanin-driven actomyosin contractility or podoplanin ligand function, we next asked whether CD44 and/or CD9 are required for FRCs to respond to CLEC-2$^+$ dendritic cells. Binding of CLEC-2^{hi} dendritic cells to FRCs drives elongation and induction of multiple protrusions, which *in vivo*, is required for acute lymph node expansion during adaptive immune responses (24, 25). FRCs respond to CLEC-2$^+$ dendritic cells *in vitro* by forming lamellipodia-like actin-rich protrusions in multiple directions (Fig. 4a), and by a reduction in F-actin stress fibres (Fig. 4c). We interpret this response as reduced actomyosin contractility, and a concurrent increase in actin polymerisation driving protrusions. This is quantified by increased morphology index (=perimeter^2/4πarea; Fig. 4d), which is predominantly driven by an increase in perimeter (Fig. 4e) rather than cell area (Fig. 4f). Strikingly, both CD44 KO and CD9 KO FRCs fail to form lamellipodia in response to dendritic cell contact (Fig. 4a). CD44 KO FRCs exhibit small protrusions with F-actin 'spikes', whereas CD9 KO FRCs attempt broader protrusions, but fail to accumulate F-actin at the leading edge (Fig. 4a). These defects are quantified by the lack of increased perimeter (Fig. 4e) and therefore also morphology index (Fig. 4d) in response to CLEC-2$^+$ dendritic cells. However, we still observe a dendritic cell-induced reduction in F-actin stress fibres in CD44 KO and CD9 KO FRCs, as well as in CD44/CD9 DKO FRCs (Fig. 4a-c), indicating that CLEC-2$^+$ dendritic cells still make contact with the FRCs and can inhibit contractility pathways, in agreement with our previous data (Fig. 2d). We conclude that both CD44 and CD9 participate in podoplanin-dependent spreading and protrusion formation via parallel, non-redundant mechanisms. Indeed, even before contact with dendritic cells, CD44 KO and CD9 KO FRCs are spread over a smaller area compared to control FRCs (Fig. 4f), suggesting that CD44 and CD9 also act to balance podoplanin-driven contractility and protrusion formation in steady state.

These data lead us to conclude that the induction of spreading and the formation of lamellipodia protrusions in response to dendritic cell contact is an active podoplanin-dependent

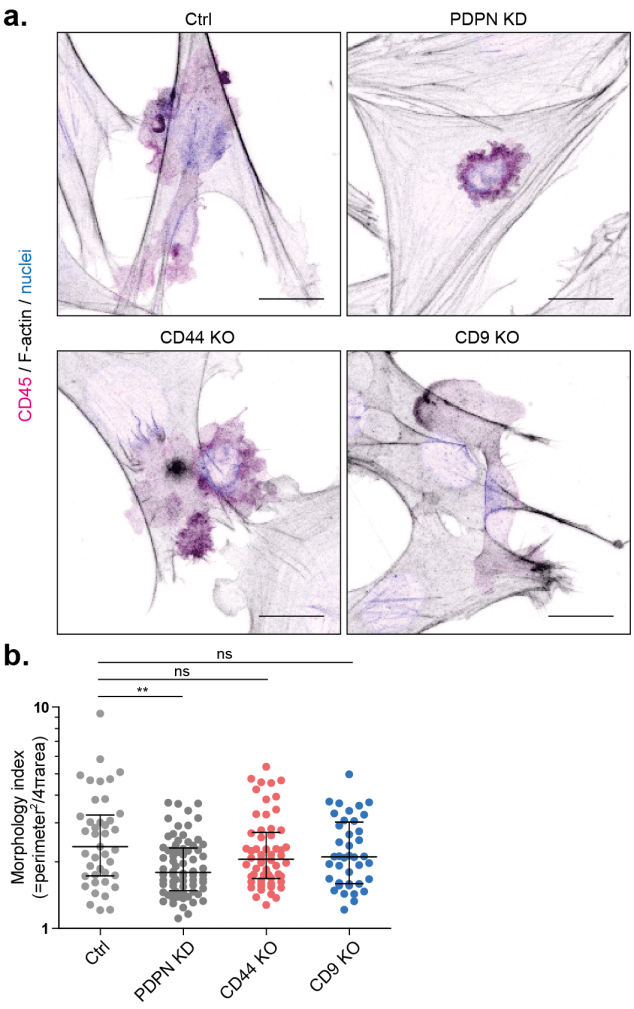

Fig. 3. Podoplanin ligand function is independent of CD44 or CD9. a. Immunofluorescence of three dimensional cultures of control (Ctrl), podoplanin siRNA knock-down (PDPN KD), CD44 knock-out (KO) or CD9 KO FRCs plus LPS-stimulated bone marrow-derived dendritic cells (CD45$^+$; magenta). Maximum Z stack projections of representative images from n=2 biological replicates are shown. The scale bars represent 20 microns. **b.** Morphology index (=perimeter^2/4πarea) of dendritic cells in interaction with an FRC. Dots represent single dendritic cells. n=40-72 dendritic cells collated from 2 biological replicates. Error bars represent median with interquartile range. $^{**}p$=0.0086. ns, not significant. Y-axis, log 10 scale.

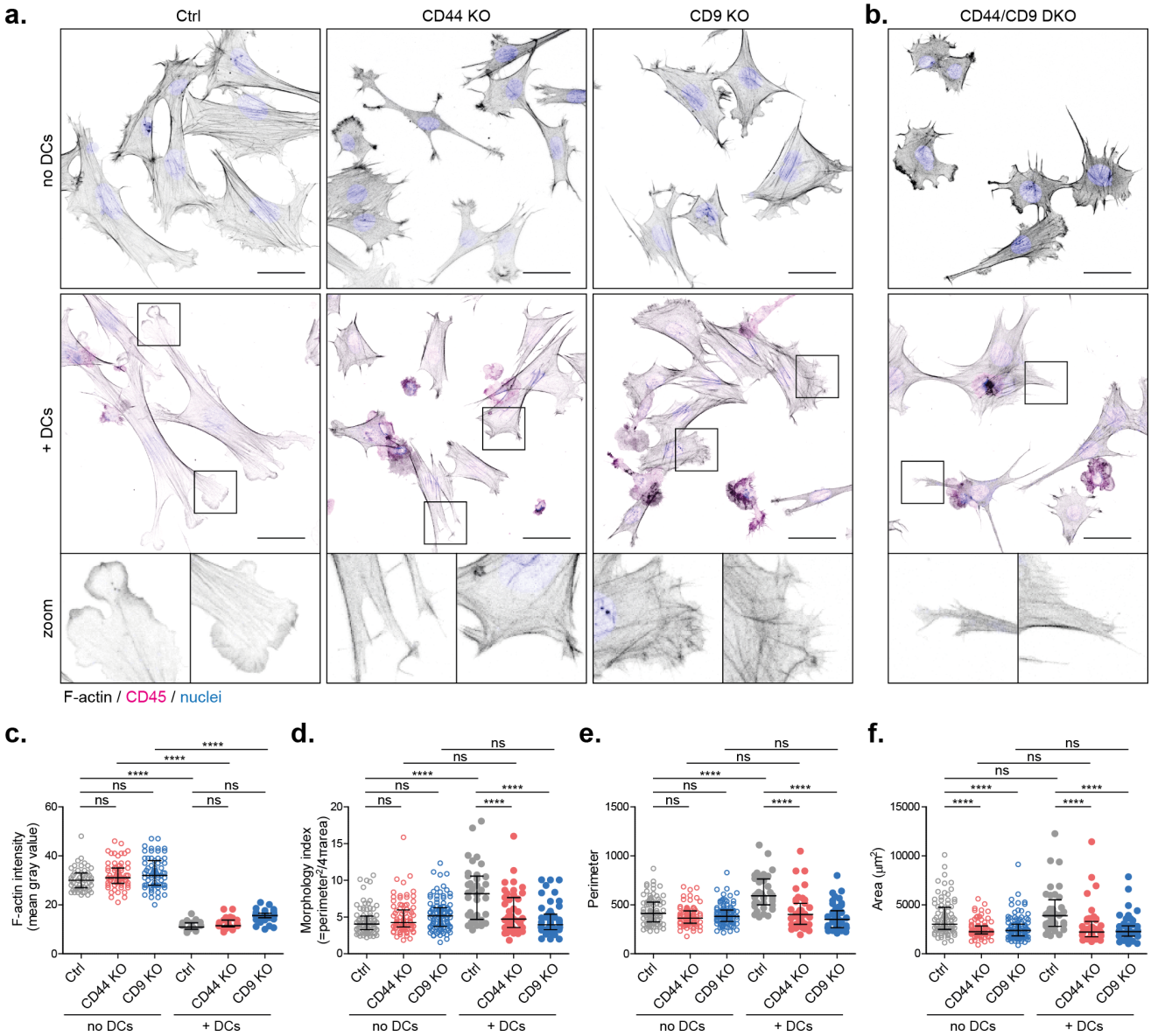

Fig. 4. CD44 and CD9 are both required for FRC spreading in response to CLEC-2$^+$ dendritic cells. a-b. Immunofluorescence of three-dimensional cultures of control (Ctrl), CD44 knock-out (KO), CD9 KO (**a**), or CD44/CD9 double-KO (DKO; **b**) FRCs without (upper row) or with (middle and bottom rows) LPS-stimulated bone marrow-derived dendritic cells (DC). Maximum Z stack projections of representative images from n=2 biological replicates are shown. The scale bars represent 50 microns. **c-f.** F-actin intensity (mean gray value of phalloidin-TRITC staining; **c**), morphology index (=perimeter^2/4πarea; **d**), perimeter (**e**), area (**f**), and of control (Ctrl, grey), CD44 KO (red) and CD9 KO (blue) FRCs alone (open circles) or in interaction with a dendritic cell (closed circles). Dots represent single FRCs. n=36-104 FRCs collated from 2 biological replicates. Error bars represent median with interquartile range. ****p<0.0001. ns, not significant.

process, and that the formation of protrusions requires both podoplanin/CD44 and podoplanin/CD9 complexes.

CD9 controls FRC-FRC interactions. We sought to determine the differential roles of CD44 and CD9 in controlling FRC morphology and phenotype in the steady state. Since both CD44 and CD9 were required for CLEC-2-induced protrusion formation, we examined Arp2/3$^+$ protrusions in CD44 KO and CD9 KO FRCs as a functional readout of actively protruding membrane. Rac1 nucleates the Arp2/3 complex, which drives formation of new actin filaments, branching from pre-existing filaments in the cortical actin network, at the leading edge of lamellipodia (51). Both CD44 KO and CD9 KO FRCs show increased membrane Arp2/3$^+$ (ARPC2) localisation in cell protrusions compared to control FRCs (Fig. 5a), but with contrasting morphology and F-actin organisation. The increase in Arp2/3$^+$ (ARPC2) staining was unexpected since both cell lines show defective protrusion formation in response to dendritic cells (Fig. 4). However, this may result from an increase in respectively podoplanin/CD44 complexes or podoplanin/CD9 complexes when the alternative binding partner is unavailable. CD44 KO FRCs exhibit small, discrete Arp2/3$^+$ protrusions, which meet and interact between neighbouring FRCs (Fig. 5a). In contrast, CD9 KO FRCs have broad Arp2/3$^+$ protrusions, covering most of the plasma membrane, and neighbouring

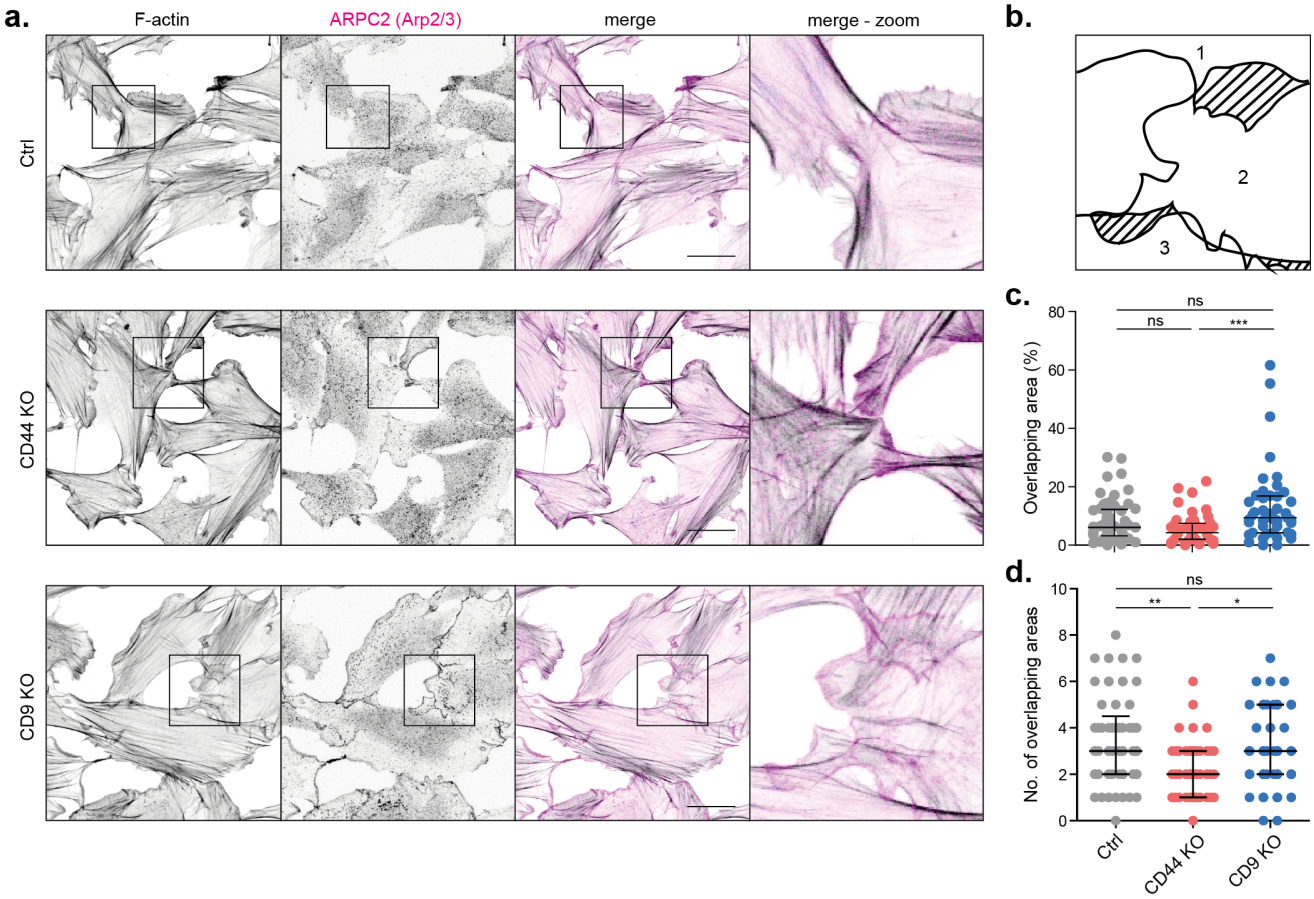

Fig. 5. CD9 controls FRC-FRC interactions. a. Immunofluorescence of Arp2/3$^+$ protrusions (magenta) in control (Ctrl, upper row), CD44 knock-out (KO; second row) and CD9 KO (bottom row) FRCs. Maximum Z stack projections of representative images from n=2 biological replicates are shown. The scale bars represent 30 microns. **b.** Schematic representation of analysis of overlapping cell areas (shaded). Individual cells are numbered. **c-d.** Percentage of total overlapping area (**c**) and number of overlapping areas (**d**) for Ctrl (grey), CD44 KO (red) and CD9 KO (blue) FRCs. Dots represent single FRCs. n=45-57 cells in total from 2 biological replicates. Error bars represent median with interquartile range. **p*=0.0295, ***p*=0.0020, ****p*=0.0003. ns, not significant.

FRCs overlap each other to a greater degree than we observe in control cultures or CD44 KO cultures (Fig. 5a-c). Furthermore, CD9 KO FRCs have a higher number of overlapping areas/cell compared to CD44 KO FRCs (Fig 5d).

Unlike other fibroblast populations which exhibit contact inhibition of locomotion (CIL) (52), repolarising and migrating away from neighbouring cells upon contact, FRCs physically connect to form an intricate multi-cellular network (24, 53–55). Network connectivity is maintained and prioritised throughout the early phases of lymph node expansion, and FRCs 'stretch' and elongate to accommodate the increasing number of proliferating lymphocytes rather than uncouple from one another (24, 25, 53). It is unknown how FRCs overcome CIL to form stable connections with their neighbours. Our data show that FRCs contact one another and overlap membranes *in vitro*, and that CD9 is necessary for FRCs to identify when and where they encounter neighbouring cells (Fig. 5). This phenotype is podoplanin-dependent, since unlike control podoplanin$^+$ FRCs, PDPN KD FRCs exhibit CIL and behave similarly to other fibroblastic cell lines, repolarising and migrating away from one another (Supplementary Fig. 2). CD9$^+$ filopodia-like protrusions (Fig. 2b) are important for sensing neighbouring cells and establishing interactions in many other biological contexts (56, 57). We suggest that CD9 expression by FRCs may facilitate podoplanin-dependent cell-cell contacts for FRC network formation *in vivo*.

Podoplanin, CD44 and CD9 are co-regulated *in vivo* during lymph node expansion. FRC spreading and elongation is a pivotal step in initiation of lymph node expansion (24, 25). This is induced by migratory CLEC-2^{hi} dendritic cells entering the lymph node, and inhibiting podoplanin-dependent actomyosin contractility in FRCs (24, 25). The lymph node is a highly structured organ consisting of different functional zones, which are organised and defined by different FRC subsets (58, 59). CLEC-2^{hi} migratory dendritic cells will first come in contact with marginal reticular cells (MRCs), a subset of FRCs defined by expression of MAdCAM-1, located below the subcapsular sinus and in the interfollicular regions (60). MRCs play an important role in lymph node development, antigen transport to the B-cell follicles, and plasma B-cell homeostasis, and provide a niche for subcapsular sinus macrophages (60–65). Furthermore, MRCs are suggested to play a role in dendritic cell transmigration from the subcapsular sinus to the T-cell zone (66). In

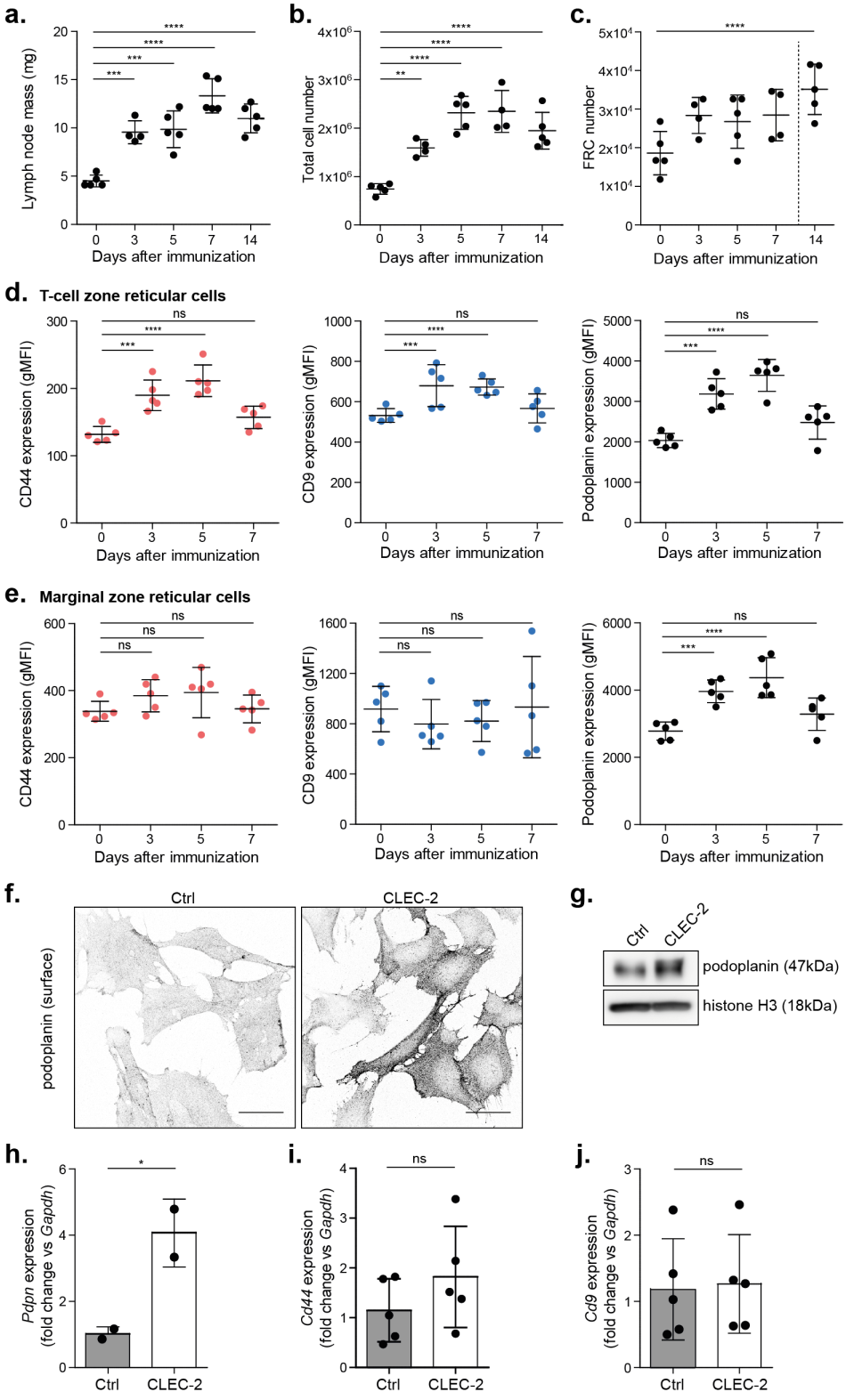

Fig. 6. Podoplanin, CD44 and CD9 expression on FRCs increases upon in vivo immunisation. a. Mass (in mg) of dissected lymph nodes. **b-e.** Analysis by flow cytometry of cell suspensions of inguinal lymph nodes from C57BL/6 mice immunized with IFA/OVA for indicated time points. FRC population was based on total lymph node cell count x (percentage of live cells) x (percentage of CD45$^-$ cells). Gating strategy is included in Supplementary Figure 5. **b.** Total live cell number based on counting beads and live-dead staining as measured by flow cytometry. **c.** FRC number. Dashed line separates FRC spreading (left) from FRC proliferation (right) phase. **d-e.** CD44 (left), CD9 (middle) and podoplanin (right) surface expression on T-zone reticular cells (TRC; podoplanin$^+$CD31$^-$MAdCAM-1$^-$; **d**) or on marginal reticular cells (MRC; podoplanin$^+$CD31$^-$MAdCAM-1$^+$; **e**). **a-e.** n=4-5 mice per time point. *p<0.05, **p<0.01, ****p<0.0001, ns, not significant. gMFI, geometric mean fluorescence intensity. **f.** Immunofluorescence of podoplanin surface expression on control (Ctrl) or CLEC-2-Fc-expressing FRC cell lines. Maximum Z stack projections of representative images from n=3 biological replicates are shown. The scale bars represent 50 microns. **g.** Western blot analysis of total podoplanin (PDPN) expression in Ctrl or CLEC-2-Fc-expressing FRC cell lines. Histone H3 was used as loading control. Representative data from n=3 biological replicates is shown. Blot is cropped to provide clear and concise presentation of results. **h-j.** *Pdpn* (**h**), *Cd44* (**i**), and *Cd9* (**j**) mRNA expression Ctrl (grey) or CLEC-2-Fc-expressing (white) FRCs. mRNA expression of gene of interest is calculated as fold change of *Gapdh* expression. Data shown as meanwith dots representing n=2-5 biological replicates. *p=0.0272. ns, not significant.

the T-cell zone, CLEC-2^{hi} migratory dendritic cells will interact with podoplanin-expressing T-cell zone FRCs (TRCs). It is unclear how MRCs alter their behaviour during lymph node expansion, but TRCs must certainly endure and adapt to the pressure of expanding T-cell populations rapidly requiring additional space.

To investigate the role of CD44 and CD9 in FRC spreading *in vivo*, we immunized mice with IFA/OVA and examined the phenotype of both MRCs and TRCs during a time course of lymph node expansion. Despite a rapid increase in lymph node size (Fig. 7a) and total cellularity (Fig. 7b), FRC numbers do not significantly increase in the first week post-immunization (Fig. 7c), indicative of the acute spreading phase of lymph node expansion, and in agreement with previous reports showing a lag in FRC proliferation (24). Within these first 5 days, CD44 and CD9 surface expression levels increase on TRCs (PDPN$^+$CD31$^-$MAdCAM-1$^-$) in parallel with podoplanin surface expression (Fig. 7d), providing further evidence for the role of partner proteins CD44 and CD9 during TRC spreading and stretching. In contrast, MRCs (PDPN$^+$CD31$^-$MAdCAM-1$^+$) do not alter surface expression of CD44 and CD9 (Fig. 7e) but do show increased podoplanin surface expression. MRCs and TRCs will experience different mechanical forces. These data indicate that the increased expression of CD44 and CD9 is required specifically by TRCs, and adds to our understanding that FRC subsets located in different lymph node microenvironments may have different phenotypes and functions.

CLEC-2 binding drives a transcriptional increase of podoplanin in FRCs. Our data showing that endogenous podoplanin levels on FRCs in lymph nodes increase during an immune response (Fig. 6d-e) is consistent with other reports (18, 25, 67), but it is unknown how this is mechanistically controlled. Both MRCs and TRCs will contact CLEC-2^{hi} migratory dendritic cells entering the lymph node (24, 25, 66), and both upregulate podoplanin expression within this early timeframe (Fig. 6d-e). We hypothesized that CLEC-2 binding, besides inhibiting podoplanin-driven actomyosin contractility, may also drive increased podoplanin expression on these FRC subsets. To model the prolonged CLEC-2 exposure from migratory dendritic cells arriving into the lymph node over several days (24, 25), we generated a CLEC-2-Fc-secreting FRC cell line (68). CLEC-2-stimulated FRCs show increased podoplanin surface expression compared to control FRCs (Fig. 6f), which cannot solely be explained by stabilisation of increased podoplanin at the plasma membrane as total cellular podoplanin protein levels are also increased (Fig. 6g). This suggests that regulation of podoplanin by CLEC-2 occurs either by inhibiting protein degradation or at the transcriptional level. Indeed we find that *Pdpn* mRNA levels are approximately 4-fold higher in CLEC-2-stimulated FRCs compared to controls (Fig. 6h). However, CLEC-2-expressing FRCs do not significantly increase *Cd44* or *Cd9* mRNA levels (Fig. 6i-j), although we do observe a trend towards higher *Cd44* expression (Fig. 6i). This is in line with RNA sequencing (RNAseq) data showing increased *Cd44* expression in response to short-term CLEC-2 stimulation (Supplementary Fig. 3). Conversely, our RNAseq data show a decrease in *Cd9* expression upon short-term CLEC-2 stimulation, but levels increase again upon longer CLEC-2 stimulation (Supplementary Fig. 3). Furthermore, both CD44 and CD9 surface levels are reduced in PDPN KD FRCs (Supplementary Fig. 3). These data indicate some level of co-regulation or co-dependence in expression of podoplanin and its membrane binding partners CD44 and CD9.

Overexpression of podoplanin drives hypercontractility *in vitro* (24, 25), yet podoplanin expression is increased during the initiation of lymph node expansion by CLEC-2 binding, when FRCs are spreading and elongating (Fig. 6). Our data demonstrate that podoplanin is involved in both contractility and spreading/protrusion pathways, and that these opposing functions are regulated by the balance of interactions with its partner proteins (Supplementary Fig. 4). CD44 and CD9 divert podoplanin away from driving actomyosin contractility and towards protrusion formation required during lymph node expansion.

Discussion

Podoplanin is intimately connected with cytoskeletal regulation of both contractility and protrusion formation, yet in FRCs neither of these processes is coupled to cell migration (1, 17). It had been assumed that FRC spreading is an indirect event in response to inhibition of actomyosin contractility (24, 25), but we now identify loss of actomyosin contractility and spreading as two differently regulated, but linked active processes (Supplementary Fig. 4). Contact with CLEC-2^{hi} dendritic cells switches function of podoplanin away from contractility and towards protrusion formation, shifting the balance towards FRC spreading. For podoplanin to drive protrusions, its membrane binding partners CD44 and tetraspanin CD9 are both required. This system whereby one protein can transiently switch functions, allows for the dynamic and rapid tissue remodelling necessary in reactive lymphoid tissue.

Overexpression of podoplanin can drive actomyosin hypercontractility (24), and as such podoplanin function needs to be tightly regulated. We show that surface expression of CD44 or CD9, or binding to CLEC-2$^+$ dendritic cells is able to counterbalance podoplanin-driven contractility. CD44/podoplanin and CD9/podoplanin complexes are both required to promote protrusion formation in response to dendritic cell contact, and function non-redundantly; CD44/podoplanin promoting lamellipodia-like and CD9/podoplanin promoting filopodia-like protrusive activity, respectively. These two pools of podoplanin complexes act in synergy for FRC spreading. The cytoplasmic tail of podoplanin interacts with ERM family member ezrin (24, 25, 36). CLEC-2 binding to podoplanin inhibits actomyosin contractility, uncouples podoplanin from ezrin, and drives podoplanin localisation to cholesterol-enriched domains (24). CD44 is also known to reside in cholesterol-enriched domains (41), and to bind ERM proteins (69). It has recently been suggested that not the ectodomain of

podoplanin (33), but its transmembrane or cytoplasmic domains are required to bind CD44 (1). This, together with our data, supports the hypothesis that CLEC-2 binding drives the localisation and interaction of podoplanin and CD44 in cholesterol-rich domains. It is currently unknown if CLEC-2-mediated clustering of podoplanin and CD44 forces uncoupling of ERM proteins, or if dephosphorylation and uncoupling of ERM proteins by an unknown mechanism provides space for clustering of podoplanin/CD44 complexes. Further studies are required to identify the specific cascade of signalling events downstream the CLEC-2/podoplanin axis. Our data suggest that the function of podoplanin would be determined not only by expression level or subcellular localisation, but by the availability of its membrane binding partners CD44 and CD9; and that the ratio between podoplanin and these binding partners control podoplanin function, balancing actomyosin contractility and protrusion formation.

Tetraspanins are membrane-organizing proteins controlling expression of surface proteins via direct interaction or as chaperone during intracellular trafficking (46). Tetraspanins control a variety of cellular processes, including cell-cell interactions, cell migration, and signalling events (38, 39). We find that tetraspanin CD82 is essential for podoplanin membrane localisation in FRCs; a more dramatic phenotype than reported in CD82 KO osteoclasts which also showed reduced podoplanin expression (42). Our data suggests that CD82 controls podoplanin trafficking to the plasma membrane. Interestingly, co-expression of podoplanin (8) and CD82 (70) is also reported in rheumatoid arthritis-associated synovial fibroblasts, suggesting CD82 may be required for podoplanin trafficking in many different tissues. It is currently unknown if CD82 is a direct partner of podoplanin, or binds indirectly via another podoplanin-partner protein. We further describe a role for tetraspanin CD9 in controlling podoplanin expression and function in FRCs. We suggest that CD9 stabilizes a portion of podoplanin molecules at the plasma membrane. In several cell types, CD9 is important for migration (71). However, our data indicate that in FRCs, CD9 is involved filopodial protrusions, impacting the connections with neighbouring cells. In the lymph node, FRCs form an intricate network in which the cells function together as a coordinated population and not as individual cells (54, 55). We hypothesize that CD9 contributes to the formation and preservation of the FRC network.

FRCs shape lymph node architecture (58). Different phenotypically distinct FRC subsets are identified based on their tissue localization and function within the lymph node (59, 63). The FRC network is especially important in controlling lymph node size (24, 25, 53). During an immune response, proliferating T cells provide a mechanical strain for T-zone FRCs (TRCs) (18), and TRC elongation and spreading is required to preserve network connectivity and stromal architecture, in advance of their proliferation. Lymph node expansion is a transient and reversible process, a cycle of remodelling through each adaptive immune response. TRCs must control the balance between actomyosin contractility and spreading/protrusion to support lymph node structure, and adapt and respond to the changing number of lymphocytes within the tissue. We suggest that podoplanin expression by TRCs is key to the adaptable phenotype of this key stromal population. We hypothesize that during homeostasis lymph node size remains stable via tonic CLEC-2 signalling provided by resident and migratory dendritic cells maintaining the balance between contraction and protrusion. During immune responses, when lymphocytes will proliferate and the lymph node will expand, the mechanical balance in the TRC network is transiently shifted towards elongation and protrusion by an influx of CLEC-2^{hi} migratory dendritic cells, and our data indicates that this shift requires higher expression of CD44 and CD9 on TRCs.

Our data also show that CLEC-2 binding can upregulate podoplanin expression. Podoplanin expression can also be induced in cancer and during wound healing (1, 17), and we now identify a potential mechanism to explain this phenomenon. Tumour cells and CAFs often reside in microenvironments of poorly structured vasculature and leaking blood vessels (72). Platelets express very high levels of CLEC-2 (73), and may bind to tumour cells and resident fibroblasts causing upregulation of podoplanin.

This study provides a molecular understanding of how a single protein can drive multiple functions. This predicts that podoplanin expression can be associated with a variety of phenotypes in different cell types, since podoplanin function is controlled and directed in part by the availability of molecular binding partners. Here, we have shown different functions for two known podoplanin complexes, however there may be additional binding partners which are currently unknown. Podoplanin is a potential target for drug development in inflammatory diseases and cancer. The data presented here should be considered when interpreting results of any effort to generate podoplanin 'blocking' drugs.

Materials and methods

Biological materials generated for this study are available upon request to the corresponding author with an MTA where appropriate.

Mice. Wild-type C57BL/6J mice were purchased from Charles River Laboratories. Both males and females were used for *in vivo* and *in vitro* experiments and were aged 6-10 weeks. All mice were age matched and housed in specific pathogen-free conditions. All animal experiments were reviewed and approved by the Animal and Ethical Review Board (AWERB) within University College London and approved by the UK Home Office in accordance with the Animals (Scientific Procedures) Act 1986 and the ARRIVE guidelines.

***In vivo* immunizations.** Mice were immunized via subcutaneous injection in the right flank with 100 μl of an emulsion of OVA in incomplete (IFA) Freund's adjuvant (100 μg OVA per mouse; Hooke Laboratories). Draining inguinal lymph nodes were taken for analysis by flow cytometry. Lymph nodes were digested as previously described (74), and cells

were counted using Precision Count Beads as per supplier's instructions (Biolegend), and stained for analysis by flow cytometry.

Cell culture. Control and podoplanin knockdown (PDPN KD) FRC cell lines (24), and CLEC-2-Fc expressing FRCs (68) are previously described. Podoplanin knockout (PDPN KO) FRC cell line was generated using CRISPR/Cas9 editing. Control FRC cell line (24) was transfected with pRP[CRISPR]-hCas9-U6>PDPN gRNA 1 plasmid (constructed and packaged by Vectorbuilder; vector ID: VB160517-1061kpr) using Lipofectamine 2000 Transfection Reagent (Thermo Fisher Scientific). We performed three rounds of transfection, and subsequently performed magnetic cell sorting (MACS) using MACS LD columns (Miltenyi Biotec), anti-mouse podoplanin-biotin antibody (clone 8.1.1, eBioscience, 13-5381-82), and anti-biotin microbeads (Miltenyi Biotec, 130-090-485) as per supplier's instructions to sort PDPN KO FRCs by negative selection. Complete knockout of podoplanin expression was confirmed using quantitative RT-PCR, flow cytometry and Western blot.

Doxycycline-inducible podoplanin-expressing FRCs were generated using the piggyBac transposon-based expression system (75). PDPN KO FRCs were transfected using Attractene Transfection Reagent (Qiagen) with the following three plasmids at a ratio of 1:1:1 - 1) plasmid carries the EF1A promotor, to drive the expression of Tet3g, and a puromycin resistance gene (constructed and packaged by Vectorbuilder; vector ID: VB151009-10079), 2) doxycycline-inducible plasmid carrying TRE3G, which drives the expression of murine podoplanin together with the fluorescence marker Cypet tagged to P2A which allows self-cleavage from podoplanin upon translation and a blasticidin resistance gene with mCherry for selection after transfection (constructed and packaged by Vectorbuilder; vector ID: VB151008-10006), and 3) plasmid expressing PBase (75). Transfected cells were selected with puromycin and blasticidin (both Invivogen). Cells were treated with 1 μg/ml doxycycline for 48 hours followed by MACS and flow associated cell sorting (FACS) to select for podoplanin expressing cells.

CD44 KO, CD9 KO, CD44/CD9 DKO, and CD82 KO FRCs were generated using CRISPR/Cas9 editing. Control or (podoplanin-inducible) PDPN KO FRCs were transfected using Attractene Transfection Reagent (Qiagen) with one or both of the following plasmids: pRP[CRISPR]-hCas9-U6>CD44-T3 exon 2 (constructed and packaged by Vectorbuilder; vector ID: VB180119-1369pus), pRP[CRISPR]-hCas9-U6>CD9 exon 1 (constructed and packaged by Vectorbuilder; vector ID: VB180119-1305adb), or pRP[CRISPR]-hCas9-U6>CD82-T1 exon 5 (constructed and packaged by Vectorbuilder; vector ID: vector ID VB180119-1391uky). Subsequently, CD44 KO, CD9 KO, and CD44/CD9 DKO FRCs underwent two or three rounds of FACS to obtain a full CD44 and/or CD9 KO FRC cell line, which was confirmed using flow cytometry (Fig. 2c), RT-PCR, and Western blot (data not shown). For generation of CD82 KO FRCs, a GFP expressing plasmid was co-transfected, and 3 days after transfection, GFP^+ cells were selected using FACS, and cultured in 96-well plates (1 cell per well) to obtain single cell clones. Complete knockout of CD82 expression was confirmed using RT-PCR (Supplementary Fig. 1).

FRC cell lines were cultured in high-glucose DMEM with GlutaMAX supplement (Gibco, via Thermo Fisher Scientific) supplemented with 10% fetal bovine serum (FBS; Sigma-Aldrich), 1% penicillin-streptomycin (P/S) and 1% insulin-transferrin-selenium (both Gibco, via Thermo Fisher Scientific) at 37°C, 10% CO_2, and passaged using cell dissociation buffer (Gibco, via Thermo Fisher Scientific).

Bone marrow-derived dendritic cells (BMDCs) were generated by culturing murine bone marrow cell suspensions in RPMI 1640 medium (Gibco, via Thermo Fisher Scientific) supplemented with 10% FBS, 1% P/S and 50 μM 2-mercaptoethanol (Gibco, via Thermo Fisher Scientific), and 20 ng/ml recombinant murine granulocyte-macrophage colony-stimulating factor (mGM-CSF, Peprotech, 315-03), as adapted from previously described protocols (76), at 37°C, 5% CO_2. On day 6, BMDCs were additionally stimulated with 10 ng/ml lipopolysaccharides from *E.coli* (LPS; Sigma-Aldrich, L4391-1MG) for 24 hours.

PDPN-CFP transfection. FRCs were plated in a 6-well culture plate ($5x10^4$ cells per well) one day before transfection with PDPN-CFP (Acton et al., 2012) (ratio 1:2) using Attractene transfection reagent (Qiagen) as per supplier's instructions. 48 hours post-transfection, FRCs were harvested for analysis of surface podoplanin and total PDPN-CFP expression by flow cytometry.

Dendritic cell-FRC co-cultures. FRCs (0.7×10^4 cells per well) were seeded on 24-well glass-bottomed cell culture plates (MatTek) at 37°C, 10% CO_2. After 24 hours, LPS-stimulated BMDCs (2.5×10^5 cells per well) were seeded into 3D collagen (type I, rat tail)/Matrigel matrix (both from Corning, via Thermo Fisher Scientific) supplemented with 10% minimum essential medium alpha medium (MEMalpha, Invitrogen, via Thermo Fisher Scientific) and 10% FCS (Greiner Bio-One) on top of the FRCs. Co-cultures were incubated overnight at 37°C, 10% CO_2. The next day, cultures were fixed with AntigenFix (DiaPath, via Solmedia) for 3 hours at room temperature (RT), followed by permeabilization and blocking with 2% bovine serum albumin (BSA; Sigma-Aldrich) and 0.2% Triton X-100 in phosphate-buffered saline (PBS) for 2 hours at RT. Subsequently, BMDCs were stained using rat anti-mouse CD45-AF647 (clone 30-F11, 1:250, Biolegend, 103123), and F-actin and cell nuclei were visualized using respectively phalloidin-TRITC (P1951-1MG) and 4,6-diamidino-2-phenylindole (DAPI; D9542-1MG; both 1:500 dilution, both from Sigma-Aldrich). Co-cultures were imaged on a Leica SP5 confocal microscope using HCX PL APO /1.25 40x oil lenses, and analysed using Fiji/ImageJ software. Z stacks (0.5 μm/step) were projected with ImageJ Z Project (maximum projection). Morphology index (=$\text{perimeter}^2/4\pi\text{area}$) was calculated using the area and perimeter of BMDCs or

FRCs by manually drawing around the cell shape using F-actin staining.

Immunofluorescence. FRCs were seeded on glass coverslips for 24 hours at 37°C, 10% CO_2. Cells were fixed in 3.6% formaldehyde (Sigma-Aldrich; diluted in PBS), and subsequently blocked in 2% BSA in PBS and stained for 1 hour at RT with the following primary mouse antibodies: rabbit anti-p34-Arc/ARPC2 (Arp2/3, 1:100, Merck, 07-227), hamster anti-podoplanin-eFluor660 (clone 8.1.1, 1:200, eBioscience, 50-5381-82), rat anti-CD44 (clone IM7, 1:200, BD Biosciences, 553131), or rat anti-CD9 (clone KMC8, 1:200, eBioscience, 14-0091-82). This was followed by incubation with appropriate Alexa Fluor-conjugated secondary antibodies (1:500, Invitrogen, via Thermo Fisher Scientific) for 1 hour at RT. F-actin and cell nuclei were visualized using respectively phalloidin-TRITC (P1951-1MG) and DAPI (D9542-1MG; both 1:500 dilution, both from Sigma-Aldrich) incubated for 15 minutes at RT, and coverslips were mounted in Mowiol (Sigma-Aldrich). Cells were imaged on a Leica SP5 confocal microscope using HCX PL APO /1.4 63x oil lenses, and analysed using Fiji/ImageJ software. Z stacks (0.5 μm/step) were projected with ImageJ Z Project (maximum projection). Proportion of contracted cells was quantified by analysing the number of contracted/blebbing cells (based on F-actin staining) compared to total number of cells per field of view.

Flow cytometry. Single-cell suspensions were incubated with FcR blocking reagent (Miltenyi Biotec) as per supplier's instructions, followed by 30 minutes staining on ice with the following primary mouse antibodies diluted in PBS supplemented with 0.5% BSA and 5mM EDTA: hamster anti-podoplanin-eFluor660 (clone 8.1.1, 1:200, eBioscience, 50-5381-82), rat anti-CD44-PE (clone IM7, 1:50, BD Biosciences, 553134), and/or rat anti-CD9-FITC (clone MZ3, 1:50, Biolegend, 124808). Stained cells were analyzed using FACSDiva software and LSR II flow cytometer (both BD Biosciences).
For analysis of lymph nodes from *in vivo* immunisations by flow cytometry, $3x10^6$ cells were incubated with purified rat IgG2b anti-mouse CD16/32 receptor antibody as per supplier's instructions (Mouse BD Fc-block, clone 2.4G2, BD Biosciences, 553141) for 20 minutes at 4C. Cells were stained with the following primary mouse antibodies (1:100 dilution) for 30 minutes at 4C: CD45-BV750 (clone 30-F11, Biolegend, 103157), CD31-PE-Cy5.5 (clone MEC 13.3, BD Biosciences, 562861), podoplanin-PE (clone 8.1.1, BD Biosciences, 566390), CD44-BV605 (clone IM7, BD Biosciences, 563058), CD9-FITC (clone MZ3, Biolegend, 124808) and MAdCAM-1-BV421 (clone MECA-367, BD Biosciences, 742812). Cells were washed with PBS and stained with Zombie Aqua fixable live-dead kit as per supplier's instructions (Biolegend, 423101) for 30 minutes at 4°C. Next, cells were fixed using Biolegend Fixation/Permeabilization Buffer as per supplier's instructions (Biolegend, 421403). Samples were analysed on BD Symphony A5 equipped with 355 nm, 405 nm, 488 nm, 561 nm and 638 nm lasers. Acquisition was set to $5x10^5$ single, live $CD45^+$ cells. FRC cell number was based on their percentage within the $CD45^-$ cells. All flow cytometry data was analysed using FlowJo Software version 10 (BD Biosciences).

Western blot. Ctrl or CLEC-2-Fc FRCs were plated in a 6-well culture plate ($1x10^5$ cells per well). After 24 hours, the culture plate was placed on ice and cells were washed twice with cold PBS. Cells were lysed in 100 μl 4x Laemmli lysis buffer (Bio-Rad) and collected using cell scraper. Samples were separated by reducing 10% SDS-polyacrylamide gel electrophoresis. Western blots were incubated with rat anti-mouse podoplanin (clone 8F11, 1:1000, Acris Antibodies, AM26513AF-N), or mouse anti-Histone H3 (1:2000, Abcam, ab24824) as loading control, in PBS supplemented with 1% skim milk powder and 0.2% BSA overnight at 4°C, followed by staining with appropriate HRP-conjugated secondary antibodies (Abcam) for 2 hours at RT. Western blots were developed using Luminata Crescendo Western HRP substrate (Merck Millipore) and imaged on ImageQuant LAS 4000 mini (GE Healthcare Life Sciences).

Transcriptome sequencing and analysis. FRCs were cultured for 24 hours, adding 50 μg/ml CLEC-2-Fc from the beginning or 6 hours before collecting cells. Control FRCs were left untreated. RNA extractions were performed using RNAeasy Kit (Qiagen) as per supplier's instructions, including a DNA digestion step to avoid genome contamination. For transcriptome sequencing and analysis, RNA preparations from FRCs were sequenced to a depth of 9 million to 22 million reads by Queen Mary University (QMUL) Genome Centre. The raw read quality control was performed by the QMUL Genome Centre using Basespace software (Illumina). Paired end FASTQ files were then aligned to Mus musculus GRCm38 reference assembly using STAR aligner software (Dobin et al., 2013). Transcripts were assembled and relative transcript abundance were calculated using Salmon software(Patro et al., 2017). Using R software (v3.4.4) and the Bioconductor tximport package (Soneson et al., 2016), transcripts per million (TPM) values were generated and annotated with ENSEMBL gene IDs. Bulk TPM data were categorised by fold change (>2 fold) between control, 6 hours and 24 hours conditions using an in-house developed R script.

RNA isolation and quantitative RT-PCR analysis. RNA lysates of Ctrl and CD82 KO FRCs were stored at -80°C until RNA isolation using RNeasy Mini kit (Qiagen) as per supplier's instructions, including a DNA digestion step to avoid genome contamination. RNA quantity and purity were determined on a NanoDrop spectrophotometer, and reverse transcribed to cDNA using SuperScript® IV First-Strand Synthesis System kit (Invitrogen, via Thermo Fisher Scientific) as per supplier's instructions. mRNA levels of *Pdpn* (transcript variant 1) or *Cd82* were determined with a CFX96 Sequence Detection System (Bio-Rad) with MESA Blue (Eurogentec, via Promega) as the fluorophore and gene-specific oligonucleotide primers. The following primers were used: *Pdpn* forward 5-CAGGGAGGGACTATAGGCGT,

Pdpn reverse 5-TGTCTGCGTTTCATCCCCTG, *Cd82* forward 5-TGGACATCATTCGCAACTACAC, *Cd82* reverse 5-GCATGGGTAAGTGGTCTTGGTA. Reaction mixtures and program conditions were applied as recommended by the manufacturer (Bio-Rad). Quantitative RT-PCR data were analyzed with the CFX Manager software (version 3.1, Bio-Rad) and checked for correct amplification and dissociation of the products. Ct values of the genes of interest were normalized to the Ct value of the housekeeping gene *Gapdh*.

Statistics. Statistical differences between two groups were determined using unpaired Student's t-test (one-tailed), or, in the case of non-Gaussian distribution, Mann-Whitney test. Statistical differences between two different parameters were determined using one-way ANOVA with Tukey's multiple comparisons test. Statistical differences between more than two groups were determined using two-way ANOVA with Tukey's multiple comparisons test, or, in the case of non-Gaussian distribution, Kruskal-Wallis test with Dunn's multiple comparisons. Statistical tests were performed using GraphPad Prism software (version 7), and differences were considered to be statistically significant at $p \leq 0.05$.

Data availability. RNAseq data (Supplementary Fig. 1 and 3) are publicly available through UCL research data repository: 10.5522/04/c.4696979.

ACKNOWLEDGEMENTS

We thank Prof Erik Sahai (The Francis Crick Institute, UK), Prof Annemiek van Spriel (RIMLS, Radboudumc, NL), Dr Louise Cramer (MRC-LMCB, UCL, UK), Dr Christopher Tape (UCL Cancer Institute, UK), and Harry Horsnell (PhD student at MRC-LMCB, UCL, UK) for critical reading of the manuscript. We thank the core staff at the UCL Cancer Institute Flow Cytometry Facility for sorting CRISPR/Cas9 edited FRC cell lines and for use of BD Symphony A5 flow cytometer. This work is supported by a Netherlands Organization for Scientific Research (NWO) Rubicon Postdoctoral Fellowship (019.162LW.004; to C.M.d.W), European Research Council Starting Grant (LNEXPANDS; to S.E.A), Cancer Research UK Career Development Fellowship (CRUK-A19763; to S.E.A) and Medical Research Council (MC-U12266B).

AUTHOR CONTRIBUTIONS C.M.d.W. and S.E.A. designed the study and wrote the manuscript; S.M. performed in vivo protein expression analysis; L.M. investigated changes in and transcriptional control of podoplanin expression upon CLEC-2; A.C.B. generated CLEC-2-Fc and (inducible) PDPN-KO FRC cell lines and assisted with cell sorting; G.C. characterized CD82 KO FRC single cell clones and investigated podoplanin expression; V.G.M. performed FRC transcriptome analysis; C.M.d.W. generated CD44 KO, CD9 KO, CD44/CD9 DKO, and CD82 KO FRC cell lines, and performed and analysed all other experiments.

Bibliography

1. Miguel Quintanilla, Lucía Montero-Montero, Jaime Renart, Ester Martín-Villar, Miguel Quintanilla, Lucía Montero-Montero, Jaime Renart, and Ester Martín-Villar. Podoplanin in Inflammation and Cancer. *International Journal of Molecular Sciences*, 20(3):707, feb 2019. ISSN 1422-0067. doi: 10.3390/ijms20030707.
2. S Breiteneder-Geleff, K Matsui, A Soleiman, P Meraner, H Poczewski, R Kalt, G Schaffner, and D Kerjaschki. Podoplanin, novel 43-kd membrane protein of glomerular epithelial cells, is down-regulated in puromycin nephrosis. *The American journal of pathology*, 151(4): 1141–52, oct 1997. ISSN 0002-9440.
3. A. Wetterwald, W. Hofstetter, M.G. Cecchini, B. Lanske, C. Wagner, H. Fleisch, and M. Atkinson. Characterization and cloning of the E11 antigen, a marker expressed by Rat Osteoblasts and Osteocytes. *Bone*, 18(2):125–132, feb 1996. ISSN 8756-3282. doi: 10.1016/8756-3282(95)00457-2.
4. Miwa Tomooka, Chiaki Kaji, Hiroshi Kojima, and Yoshihiko Sawa. Distribution of podoplanin-expressing cells in the mouse nervous systems. *Acta histochemica et cytochemica*, 46(6): 171–7, dec 2013. ISSN 0044-5991. doi: 10.1267/ahc.13035.
5. Mary C Williams, Yu Xia Cao, Anne Hinds, Arun K Rishi, and Antoinette Wetterwald. T1α Protein Is Developmentally Regulated and Expressed by Alveolar Type I Cells, Choroid Plexus, and Ciliary Epithelia of Adult Rats. *American Journal of Respiratory Cell and Molecular Biology*, 14(6):577–585, dec 1996. ISSN 10441549. doi: 10.1165/ajrcmb.14.6.8652186.
6. Francisco G. Scholl, Carlos Gamallo, Senén Vilaró, and Miguel Quintanilla. Identification of PA2.26 antigen as a novel cell-surface mucin-type glycoprotein that induces plasma membrane extensions and increased motility in keratinocytes. *Journal of Cell Science*, 112(24): 4601–4613, 1999. ISSN 00219533.
7. A G Farr, M L Berry, A Kim, A J Nelson, M P Welch, and A Aruffo. Characterization and cloning of a novel glycoprotein expressed by stromal cells in T-dependent areas of peripheral lymphoid tissues. *The Journal of experimental medicine*, 176(5):1477–82, nov 1992. ISSN 0022-1007. doi: 10.1084/jem.176.5.1477.
8. Anna Karin H. Ekwall, Thomas Eisler, Christian Anderberg, Chunsheng Jin, Niclas Karlsson, Mikael Brisslert, and Maria I Bokarewa. The tumour-associated glycoprotein podoplanin is expressed in fibroblast-like synoviocytes of the hyperplastic synovial lining layer in rheumatoid arthritis. *Arthritis Research and Therapy*, 13(2):R40, mar 2011. ISSN 14786362. doi: 10.1186/ar3274.
9. Haruhisa Kitano, Shun Ichiro Kageyama, Stephen M. Hewitt, Ryuji Hayashi, Yoshinori Doki, Yoshitomo Ozaki, Shozo Fujino, Mikiko Takikita, Hajime Kubo, and Junya Fukuoka. Podoplanin expression in cancerous stroma induces lymphangiogenesis and predicts lymphatic spread and patient survival. *Archives of Pathology and Laboratory Medicine*, 134 (10):1520–1527, 2010. ISSN 00039985.
10. Edris A.F. Mahtab, Maurits C.E.F. Wijffels, Nynke M.S. Van Den Akker, Nathan D. Hahurij, Heleen Lie-Venema, Lambertus J. Wisse, Marco C. DeRuiter, Pavel Uhrin, Jan Zaujec, Bernd R. Binder, Martin J. Schalij, Robert E. Poelmann, and Adriana C. Gittenberger-De Groot. Cardiac malformations and myocardial abnormalities inpodoplanin knockout mouse embryos: Correlation with abnormal epicardial development. *Developmental Dynamics*, 237(3):847–857, mar 2008. ISSN 10588388. doi: 10.1002/dvdy.21463.
11. Edris A.F. Mahtab, Rebecca Vicente-Steijn, Nathan D. Hahurij, Monique R.M. Jongbloed, Lambertus J. Wisse, Marco C. DeRuiter, Pavel Uhrin, Jan Zaujec, Bernd R. Binder, Martin J. Schalij, Robert E. Poelmann, and Adriana C. Gittenberger-De Groot. Podoplanin deficient mice show a rhoa-related hypoplasia of the sinus venosus myocardium including the sinoatrial node. *Developmental Dynamics*, 238(1):183–193, jan 2009. ISSN 10588388. doi: 10.1002/dvdy.21819.
12. Maria I Ramirez, Guetchyn Millien, Anne Hinds, YuXia Cao, David C Seldin, and Mary C Williams. T1α, a lung type I cell differentiation gene, is required for normal lung cell proliferation and alveolus formation at birth. *Developmental Biology*, 256(1):62–73, apr 2003. ISSN 0012-1606. doi: 10.1016/S0012-1606(02)00098-2.
13. Vivien Schacht, Maria I. Ramirez, Young Kwon Hong, Satoshi Hirakawa, Dian Feng, Natasha Harvey, Mary Williams, Ann M. Dvorak, Harold F. Dvorak, Guillermo Oliver, and Michael Detmar. T1alpha/podoplanin deficiency disrupts normal lymphatic vasculature formation and causes lymphedema. *EMBO Journal*, 22(14):3546–3556, 2003. ISSN 02614189. doi: 10.1093/emboj/cdg342.
14. Katsue Suzuki-Inoue, Osamu Inoue, Guo Ding, Satoshi Nishimura, Kazuya Hokamura, Koji Eto, Hirokazu Kashiwagi, Yoshiaki Tomiyama, Yutaka Yatomi, Kazuo Umemura, Yonchol Shin, Masanori Hirashima, and Yukio Ozaki. Essential in vivo roles of the C-type lectin receptor CLEC-2: embryonic/neonatal lethality of CLEC-2-deficient mice by blood/lymphatic misconnections and impaired thrombus formation of CLEC-2-deficient platelets. *The Journal of biological chemistry*, 285(32):24494–507, aug 2010. ISSN 1083-351X. doi: 10.1074/jbc.M110.130575.
15. Masaru Honma, Masako Minami-Hori, Hidetoshi Takahashi, and Hajime Iizuka. Podoplanin expression in wound and hyperproliferative psoriatic epidermis: Regulation by TGF-β and STAT-3 activating cytokines, IFN-γ, IL-6, and IL-22. *Journal of Dermatological Science*, 65 (2):134–140, feb 2012. ISSN 0923-1811. doi: 10.1016/J.JDERMSCI.2011.11.011.
16. Jessica R. Hitchcock, Charlotte N. Cook, Saeeda Bobat, Ewan A. Ross, Adriana Flores-Langarica, Kate L. Lowe, Mahmood Khan, C. Coral Dominguez-Medina, Sian Lax, Manuela Carvalho-Gaspar, Stefan Hubscher, G. Ed Rainger, Mark Cobbold, Christopher D. Buckley, Tim J. Mitchell, Andrea Mitchell, Nick D. Jones, N. Van Rooijen, Daniel Kirchhofer, Ian R. Henderson, David H. Adams, Steve P. Watson, and Adam F. Cunningham. Inflammation drives thrombosis after Salmonella infection via CLEC-2 on platelets. *Journal of Clinical Investigation*, 125(12):4429–4446, 2015. ISSN 15588238. doi: 10.1172/JCI79070.
17. Jillian L Astarita, Sophie E Acton, and Shannon J Turley. Podoplanin: emerging functions in development, the immune system, and cancer. *Frontiers in immunology*, 3(September): 283, jan 2012. ISSN 1664-3224. doi: 10.3389/fimmu.2012.00283.
18. Chen-Ying Yang, Tobias K Vogt, Stéphanie Favre, Leonardo Scarpellino, Hsin-Ying Huang, Fabienne Tacchini-Cottier, and Sanjiv A Luther. Trapping of naive lymphocytes triggers rapid growth and remodeling of the fibroblast network in reactive murine lymph nodes. *Proceedings of the National Academy of Sciences of the United States of America*, 111(1):E109–18, 2014. ISSN 1091-6490. doi: 10.1073/pnas.1312585111.
19. Shubham Pandey, Frédéric Mourcin, Tony Marchand, Saba Nayar, Marion Guirriec, Céline Pangault, Céline Monvoisin, Patricia Amé-Thomas, Fabien Guilloton, Joelle Dulong, Mark Coles, Thierry Fest, Anja Mottok, Francesca Barone, and Karin Tarte. IL-4/CXCL12 loop is a key regulator of lymphoid stroma function in follicular lymphoma. *Blood*, 129(18):2507–2518, may 2017. ISSN 1528-0020. doi: 10.1182/blood-2016-08-737239.
20. Moritz Durchdewald, Juan Guinea-Viniegra, Daniel Haag, Astrid Riehl, Peter Lichter, Meinhard Hahn, Erwin F Wagner, Peter Angel, and Jochen Hess. Podoplanin is a novel fos target gene in skin carcinogenesis. *Cancer Research*, 68(17):6877–6883, sep 2008. ISSN 00085472. doi: 10.1158/0008-5472.CAN-08-0299.
21. Akiko Kunita, Takeshi G. Kashima, Atsushi Ohazama, Agamemnon E. Grigoriadis, and Masashi Fukayama. Podoplanin Is Regulated by AP-1 and Promotes Platelet Aggregation and Cell Migration in Osteosarcoma. *The American Journal of Pathology*, 179(2):1041–1049, aug 2011. ISSN 0002-9440. doi: 10.1016/J.AJPATH.2011.04.027.
22. Heike Peterziel, Julia Müller, Andreas Danner, Sebastian Barbus, Hai Kun Liu, Bernhard Radlwimmer, Torsten Pietsch, Peter Lichter, Günther Schütz, Jochen Hess, and Peter Angel. Expression of podoplanin in human astrocytic brain tumors is controlled by the PI3K-AKT-AP-1 signaling pathway and promoter methylation. *Neuro-Oncology*, 14(4):426–439, apr 2012. ISSN 15228517. doi: 10.1093/neuonc/nos055.
23. Young-Kwon Hong, Natasha Harvey, Yun-Hee Noh, Vivien Schacht, Satoshi Hirakawa, Michael Detmar, and Guillermo Oliver. Prox1 is a master control gene in the program specifying lymphatic endothelial cell fate. *Developmental Dynamics*, 225(3):351–357, nov 2002.

ISSN 1058-8388. doi: 10.1002/dvdy.10163.

24. Sophie E. Acton, Aaron J. Farrugia, Jillian L. Astarita, Diego Mourão-Sá, Robert P. Jenkins, Emma Nye, Steven Hooper, Janneke van Blijswijk, Neil C. Rogers, Kathryn J. Snelgrove, Ian Rosewell, Luis F. Moita, Gordon Stamp, Shannon J. Turley, Erik Sahai, and Caetano Reis e Sousa. Dendritic cells control fibroblastic reticular network tension and lymph node expansion. *Nature*, 514(7523):498–502, oct 2014. ISSN 0028-0836. doi: 10.1038/nature13814.
25. Jillian L Astarita, Viviana Cremasco, Jianxin Fu, Max C Darnell, James R Peck, Janice M Nieves-Bonilla, Kai Song, Yuji Kondo, Matthew C Woodruff, Alvin Gogineni, Lucas Onder, Burkhard Ludewig, Robby M Weimer, Michael C Carroll, David J Mooney, Lijun Xia, and Shannon J Turley. The CLEC-2-podoplanin axis controls the contractility of fibroblastic reticular cells and lymph node microarchitecture. *Nature immunology*, 16(1):75–84, 2015. ISSN 1529-2916. doi: 10.1038/ni.3035.
26. Brett H Herzog, Jianxin Fu, Stephen J Wilson, Paul R Hess, Aslihan Sen, J. Michael McDaniel, Yanfang Pan, Minjia Sheng, Tadayuki Yago, Robert Silasi-Mansat, Samuel McGee, Frauke May, Bernhard Nieswandt, Andrew J Morris, Florea Lupu, Shaun R Coughlin, Rodger P. McEver, Hong Chen, Mark L Kahn, and Lijun Xia. Podoplanin maintains high endothelial venule integrity by interacting with platelet CLEC-2. *Nature*, 502(7469):105–9, oct 2013. ISSN 1476-4687. doi: 10.1038/nature12501.
27. Cécile Bénézech, Saba Nayar, Brenda a. Finney, David R. Withers, Kate Lowe, Guillaume E. Desanti, Clare L. Marriott, Steve P. Watson, Jorge H. Caamaño, Christopher D. Buckley, and Francesca Barone. CLEC-2 is required for development and maintenance of lymph nodes. *Blood*, 123:3200–3207, 2014. ISSN 15280020. doi: 10.1182/blood-2013-03-489286.
28. Leah N. Cueni and Michael Detmar. Galectin-8 interacts with podoplanin and modulates lymphatic endothelial cell functions. *Experimental Cell Research*, 315(10):1715–1723, jun 2009. ISSN 0014-4827. doi: 10.1016/J.YEXCR.2009.02.021.
29. Takashi Shibuya, Masaru Honma, Mizue Fujii, Shin Iinuma, and Akemi Ishida-Yamamoto. Podoplanin suppresses the cell adhesion of epidermal keratinocytes via functional regulation of β1-integrin. *Archives of Dermatological Research*, 311(1):45–53, nov 2019. ISSN 1432069X. doi: 10.1007/s00403-018-1878-9.
30. Lewis S C Ward, Lozan Sheriff, Jennifer L Marshall, Julia E Manning, Alexander Brill, Gerard B Nash, and Helen M McGettrick. Podoplanin regulates the migration of mesenchymal stromal cells and their interaction with platelets. *Journal of cell science*, 132(5):jcs.222067, feb 2019. ISSN 1477-9137. doi: 10.1242/jcs.222067.
31. Jaroslaw Suchanski, Anna Tejchman, Maciej Zacharski, Aleksandra Piotrowska, Jedrzej Grzegrzolka, Grzegorz Chodaczek, Katarzyna Nowinska, Janusz Rys, Piotr Dziegiel, Claudine Kieda, and Maciej Ugorski. Podoplanin increases the migration of human fibroblasts and affects the endothelial cell network formation: A possible role for cancer-associated fibroblasts in breast cancer progression. *PLOS ONE*, 12(9):e0184970, sep 2017. ISSN 1932-6203. doi: 10.1371/journal.pone.0184970.
32. Andreas Wicki, François Lehembre, Nikolaus Wick, Brigitte Hantusch, Dontscho Kerjaschki, and Gerhard Christofori. Tumor invasion in the absence of epithelial-mesenchymal transition: Podoplanin-mediated remodeling of the actin cytoskeleton. *Cancer Cell*, 9(4):261–272, 2006. ISSN 15356108. doi: 10.1016/j.ccr.2006.03.010.
33. E Martín-Villar, B Fernández-Muñoz, M Parsons, MM Yurrita, D Megías, E Pérez-Gómez, GE Jones, and M Quintanilla. Podoplanin Associates with CD44 to Promote Directional Cell Migration. *Mol Biol Cell*, 21(24):4387–99, 2010. doi: 10.1091/mbc.E10-06-0489.
34. Akiko Kunita, Vanessa Baeriswyl, Claudia Meda, Erik Cabuy, Kimiko Takeshita, Enrico Giraudo, Andreas Wicki, Masashi Fukayama, and Gerhard Christofori. Inflammatory Cytokines Induce Podoplanin Expression at the Tumor Invasive Front. *American Journal of Pathology*, 188(5):1276–1288, feb 2018. ISSN 15252191. doi: 10.1016/j.ajpath.2018.01.016.
35. E Martín-Villar, B Borda-d'Agua, P Carrasco-Ramirez, J Renart, M Parsons, M Quintanilla, and G E Jones. Podoplanin mediates ECM degradation by squamous carcinoma cells through control of invadopodia stability. *Oncogene*, 34(October):4531–4544, aug 2015. ISSN 1476-5594. doi: 10.1038/onc.2014.388.
36. Ester Martín-Villar, Diego Megías, Susanna Castel, Maria Marta Yurrita, Senén Vilaró, and Miguel Quintanilla. Podoplanin binds ERM proteins to activate RhoA and promote epithelial-mesenchymal transition. *Journal of Cell Science*, 119(21):4541–4553, 2006. doi: 10.1242/jcs.03218.
37. Ester Martín-Villar, Francisco G. Scholl, Carlos Gamallo, Maria M. Yurrita, Mario Muñoz-Guerra, Jesús Cruces, and Miguel Quintanilla. Characterization of human PA2.26 antigen (T1α-2, podoplanin), a small membrane mucin induced in oral squamous cell carcinomas. *International Journal of Cancer*, 113(6):899–910, mar 2005. ISSN 00207136. doi: 10.1002/ijc.20656.
38. Sjoerd J. van Deventer, Vera Marie E Dunlock, and Annemiek B. van Spriel. Molecular interactions shaping the tetraspanin web. *Biochemical Society Transactions*, 45(3):741–750, 2017. ISSN 0300-5127. doi: 10.1042/BST20160284.
39. Christina M. Termini and Jennifer M. Gillette. Tetraspanins Function as Regulators of Cellular Signaling. *Frontiers in cell and developmental biology*, 5:34, apr 2017. ISSN 2296-634X. doi: 10.3389/fcell.2017.00034.
40. Youya Nakazawa, Shigeo Sato, Mikihiko Naito, Yukinari Kato, Kazuhiko Mishima, Hiroyuki Arai, Takashi Tsuruo, and Naoya Fujita. Tetraspanin family member CD9 inhibits Aggrus/podoplanin-induced platelet aggregation and suppresses pulmonary metastasis. *Blood*, 112(5):1730–1739, 2008. ISSN 00064971. doi: 10.1182/blood-2007-11-124693.
41. Beatriz Fernández-Muñoz, María M. Yurrita, Ester Martín-Villar, Patricia Carrasco-Ramírez, Diego Megías, Jaime Renart, and Miguel Quintanilla. The transmembrane domain of podoplanin is required for its association with lipid rafts and the induction of epithelial-mesenchymal transition. *International Journal of Biochemistry and Cell Biology*, 43(6):886–896, 2011. ISSN 13572725. doi: 10.1016/j.biocel.2011.02.010.
42. Alexis Bergsma, Sourik S. Ganguly, Mollie E. Wiegand, Daniel Dick, Bart O. Williams, and Cindy K. Miranti. Regulation of cytoskeleton and adhesion signaling in osteoclasts by tetraspanin CD82. *Bone Reports*, 10:100196, jun 2019. ISSN 23521872. doi: 10.1016/j.bonr.2019.100196.
43. Wei M Liu, Feng Zhang, Simon Moshiach, Bin Zhou, Chao Huang, Kamalakkannan Srinivasan, Seema Khurana, Yi Zheng, Jill M Lahti, and Xin A Zhang. Tetraspanin CD82 Inhibits Protrusion and Retraction in Cell Movement by Attenuating the Plasma Membrane- Dependent Actin Organization. *Plos One*, 7(12):e51797, 2012. doi: 10.1371/journal.pone.0051797.
44. Alix Delaguillaumie, Cécile Lagaudrière-Gesbert, Michel R Popoff, and Hélène Conjeaud. Rho GTPases link cytoskeletal rearrangements and activation processes induced via the tetraspanin CD82 in T lymphocytes. *Journal of Cell Science*, 115:433–443, 2002.
45. E. L. Jones, J. L. Wee, M. C. Demaria, J. Blakeley, P. K. Ho, J. Vega-Ramos, J. A. Villadangos, A. B. van Spriel, M. J. Hickey, G. J. Hammerling, and M. D. Wright. Dendritic Cell Migration and Antigen Presentation Are Coordinated by the Opposing Functions of the Tetraspanins CD82 and CD37. *The Journal of Immunology*, 196(3):978–87, 2016. ISSN 0022-1767. doi: 10.4049/jimmunol.1500357.
46. F Berditchevski and E Odintsova. Tetraspanins as regulators of protein trafficking. *Traffic*, 8 (2):89–96, 2007.
47. Brandon Zimmerman, Brian McMillan, Tom Seegar, Andrew Kruse, and Stephen Blacklow. Crystal Structure of Human Tetraspanin CD81 Reveals a Conserved Intramembrane Binding Cavity. *The FASEB Journal*, 30(1 Supplement):lb71–lb71, 2016. ISSN 0892-6638. doi: 10.1016/j.cell.2016.09.056.
48. Sophie E Acton, Jillian L Astarita, Deepali Malhotra, Veronika Lukacs-Kornek, Bettina Franz, Paul R Hess, Zoltan Jakus, Michael Kuligowski, Anne L Fletcher, Kutlu G Elpek, Angelique Bellemare-Pelletier, Lindsay Sceats, Erika D Reynoso, Santiago F Gonzalez, Daniel B Graham, Jonathan Chang, Anneli Peters, Matthew Woodruff, Young-A Kim, Wojciech Swat, Takashi Morita, Vijay Kuchroo, Michael C Carroll, Mark L Kahn, Kai W Wucherpfennig, and Shannon J Turley. Podoplanin-rich stromal networks induce dendritic cell motility via activation of the C-type lectin receptor CLEC-2. *Immunity*, 37(2):276–89, aug 2012. ISSN 1097-4180. doi: 10.1016/j.immuni.2012.05.022.
49. Diego Mourão-Sá, Matthew J Robinson, Santiago Zelenay, David Sancho, Probir Chakravarty, Rasmus Larsen, Maud Plantinga, Nico Van Rooijen, Miguel P Soares, Bart Lambrecht, Caetano Reis e Sousa, Diego Moura, David Sancho, Probir Chakravarty, Rasmus Larsen, Maud Plantinga, Nico Van Rooijen, Miguel P Soares, and Bart Lambrecht. CLEC-2 signaling via Syk in myeloid cells can regulate inflammatory responses. *European journal of immunology*, 41(10):3040–53, oct 2011. ISSN 1521-4141. doi: 10.1002/eji.201141641.
50. Charlotte M de Winde, Alexandra L Matthews, Sjoerd van Deventer, Alie van der Schaaf, Neil D Tomlinson, Jing Yang, Erik Jansen, Johannes A Eble, Bernhard Nieswandt, Helen M McGettrick, Carl G Figdor, Sophie E Acton, Michael G Tomlinson, and Annemiek B van Spriel. C-type lectin-like receptor 2 (CLEC-2)-dependent DC migration is controlled by tetraspanin CD37. *Journal of cell science*, 131(19):jcs214551, sep 2018. doi: 10.1242/jcs.214551.
51. Klemens Rottner and Matthias Schaks. Assembling actin filaments for protrusion. *Current Opinion in Cell Biology*, 56:53–63, feb 2019. ISSN 0955-0674. doi: 10.1016/J.CEB.2018.09.004.
52. Alice Roycroft and Roberto Mayor. Molecular basis of contact inhibition of locomotion. *Cellular and Molecular Life Sciences*, 73(6):1119–1130, mar 2016. ISSN 14209071. doi: 10.1007/s00018-015-2090-0.
53. Alexander Link, Tobias K. Vogt, Stéphanie Favre, Mirjam R. Britschgi, Hans Acha-Orbea, Boris Hinz, Jason G. Cyster, and Sanjiv A. Luther. Fibroblastic reticular cells in lymph nodes regulate the homeostasis of naive T cells. *Nature Immunology*, 8(11):1255–1265, 2007. ISSN 1529-2908. doi: 10.1038/ni1513.
54. Mario Novkovic, Lucas Onder, Jovana Cupovic, Jun Abe, David Bomze, Viviana Cremasco, Elke Scandella, Jens V. Stein, Gennady Bocharov, Shannon J. Turley, and Burkhard Ludewig. Topological Small-World Organization of the Fibroblastic Reticular Cell Network Determines Lymph Node Functionality. *PLOS Biology*, 14(7):e1002515, jul 2016. ISSN 1545-7885. doi: 10.1371/journal.pbio.1002515.
55. Kasper M W Soekarjo, Johannes Textor, and Rob J de Boer. Local Attachment Explains Small World–like Properties of Fibroblastic Reticular Cell Networks in Lymph Nodes. *The Journal of Immunology*, 202(11):3318–3325, apr 2019. ISSN 0022-1767. doi: 10.4049/jimmunol.1801016.
56. Keisuke Kaji, Shoji Oda, Tomohide Shikano, Tatsuya Ohnuki, Yoshikatsu Uematsu, Junko Sakagami, Norihiro Tada, Shunichi Miyazaki, and Akira Kudo. The gamete fusion process is defective in eggs of Cd9-deficient mice. *Nature Genetics*, 24(3):279–282, mar 2000. ISSN 1061-4036. doi: 10.1038/73502.
57. Raquel Reyes, Beatriz Cardeñes, Yesenia Machado-Pineda, and Carlos Cabañas. Tetraspanin CD9: A key regulator of cell adhesion in the immune system, apr 2018. ISSN 16643224.
58. Anne L Fletcher, Sophie E Acton, and Konstantin Knoblich. Lymph node fibroblastic reticular cells in health and disease. *Nature reviews. Immunology*, 15(6):350–361, 2015. ISSN 1474-1741. doi: 10.1038/nri3846.
59. Lauren B Rodda, Erick Lu, Mariko L Bennett, Caroline L Sokol, Xiaoming Wang, Sanjiv A Luther, Ben A Barres, Andrew D Luster, Chun Jimmie Ye, and Jason G Cyster. Single-Cell RNA Sequencing of Lymph Node Stromal Cells Reveals Niche-Associated Heterogeneity. *Immunity*, 48(5):1014–1028.e6, apr 2018. ISSN 1097-4180. doi: 10.1016/j.immuni.2018.04.006.
60. Tomoya Katakai, Hidenori Suto, Manabu Sugai, Hiroyuki Gonda, Atsushi Togawa, Sachiko Suematsu, Yukihiko Ebisuno, Koko Katagiri, Tatsuo Kinashi, and Akira Shimizu. Organizer-like reticular stromal cell layer common to adult secondary lymphoid organs. *Journal of immunology (Baltimore, Md. : 1950)*, 181(9):6189–200, nov 2008. ISSN 1550-6606. doi: 10.4049/jimmunol.181.9.6189.
61. Marc Bajénoff and Ronald N. Germain. B-cell follicle development remodels the conduit system and allows soluble antigen delivery to follicular dendritic cells. *Blood*, 114(24):4989–4997, dec 2009. ISSN 0006-4971. doi: 10.1182/BLOOD-2009-06-229567.
62. Ramon Roozendaal, Thorsten R Mempel, Lisa a Pitcher, F Santiago, Admar Verschoor, Reina E Mebius, Ulrich H Von Andrian, and C Michael. Conduits Mediate Transport of Low Molecular Weight Antigen to Lymph Node Follicles. *Immunity*, 30(2):264–276, 2010. doi: 10.1016/j.immuni.2008.12.014.Conduits.
63. Di Huang, Jianing Chen, Linbin Yang, Qian Ouyang, Jiaqian Li, Liyan Lao, Jinghua Zhao, Jiang Liu, Yiwen Lu, Yue Xing, Fei Chen, Fengxi Su, Herui Yao, Qiang Liu, Shicheng Su, and Erwei Song. NKILA lncRNA promotes tumor immune evasion by sensitizing T cells to activation-induced cell death. *Nature Immunology*, 19(10):1112–1125, oct 2018. ISSN 15292916. doi: 10.1038/s41590-018-0207-y.

64. Isabelle Mondor, Myriam Baratin, Marine Lagueyrie, Lisa Saro, Sandrine Henri, Rebecca Gentek, Delphine Suerinck, Wolfgang Kastenmuller, Jean X Jiang, and Marc Bajénoff. Lymphatic Endothelial Cells Are Essential Components of the Subcapsular Sinus Macrophage Niche. *Immunity*, 50(6):1453–1466.e4, apr 2019. ISSN 10974180. doi: 10.1016/j.immuni.2019.04.002.
65. Abdouramane Camara, Olga G Cordeiro, Farouk Alloush, Janina Sponsel, Mélanie Chypre, Lucas Onder, Kenichi Asano, Masato Tanaka, Hideo Yagita, Burkhard Ludewig, Vincent Flacher, and Christopher G Mueller. Lymph Node Mesenchymal and Endothelial Stromal Cells Cooperate via the RANK-RANKL Cytokine Axis to Shape the Sinusoidal Macrophage Niche. *Immunity*, 50(6):1467–1481.e6, jun 2019. ISSN 1097-4180. doi: 10.1016/j.immuni.2019.05.008.
66. Tomoya Katakai. Marginal reticular cells: a stromal subset directly descended from the lymphoid tissue organizer. *Frontiers in immunology*, 3:200, 2012. ISSN 1664-3224. doi: 10.3389/fimmu.2012.00200.
67. Lucie Peduto, Sophie Dulauroy, Matthias Lochner, Gerald F Späth, Miguel A Morales, Ana Cumano, and Gérard Eberl. Inflammation recapitulates the ontogeny of lymphoid stromal cells. *Journal of immunology (Baltimore, Md. : 1950)*, 182(9):5789–99, may 2009. ISSN 1550-6606. doi: 10.4049/jimmunol.0803974.
68. Victor G Martinez, Valeriya Pankova, Lukas Krasny, Tanya Singh, Ian J. White, Agnesska C. Benjamin, Simone Dertschnig, Harry L. Horsnell, Janos Kriston-Vizi, Jemima J. Burden, Paul H. Huang, Christopher J. Tape, and Sophie Acton. Conduit Integrity is Compromised During Acute Lymph Node Expansion. *bioRxiv*, page 527481, jan 2019. doi: 10.2139/ssrn.3334979.
69. S Tsukita, K Oishi, N Sato, J Sagara, A Kawai, and S Tsukita. ERM family members as molecular linkers between the cell surface glycoprotein CD44 and actin-based cytoskeletons. *The Journal of cell biology*, 126(2):391–401, jul 1994. ISSN 0021-9525. doi: 10.1083/jcb.126.2.391.
70. Elena Neumann, Maria C Schwarz, Rebecca Hasseli, Marie-Lisa Hülser, Simon Classen, Michael Sauerbier, Stefan Rehart, and Ulf Mueller-Ladner. Tetraspanin CD82 affects migration, attachment and invasion of rheumatoid arthritis synovial fibroblasts. *Annals of the rheumatic diseases*, 77(11):1619–1626, nov 2018. ISSN 1468-2060. doi: 10.1136/annrheumdis-2018-212954.
71. Xupin Jiang, Jiaping Zhang, and Yuesheng Huang. Tetraspanins in cell migration. *Cell Adhesion and Migration*, 9(5):406–415, 2015. ISSN 19336926. doi: 10.1080/19336918.2015.1005465.
72. Marco B. Schaaf, Abhishek D. Garg, and Patrizia Agostinis. Defining the role of the tumor vasculature in antitumor immunity and immunotherapy article, feb 2018. ISSN 20414889.
73. Katsue Suzuki-Inoue, Gemma L J Fuller, Angel García, Johannes A Eble, Stefan Pöhlmann, Osamu Inoue, T Kent Gartner, Sascha C Hughan, Andrew C Pearce, Gavin D Laing, R David G Theakston, Edina Schweighoffer, Nicole Zitzmann, Takashi Morita, Victor L J Tybulewicz, Yukio Ozaki, and Steve P Watson. A novel Syk-dependent mechanism of platelet activation by the C-type lectin receptor CLEC-2. *Blood*, 107(2):542–9, jan 2006. ISSN 0006-4971. doi: 10.1182/blood-2005-05-1994.
74. Anne L. Fletcher, Deepali Malhotra, Sophie E. Acton, Veronika Lukacs-Kornek, Angelique Bellemare-Pelletier, Mark Curry, Myriam Armant, and Shannon J. Turley. Reproducible isolation of lymph node stromal cells reveals site-dependent differences in fibroblastic reticular cells. *Frontiers in Immunology*, 2(SEP):1–15, 2011. ISSN 16643224. doi: 10.3389/fimmu.2011.00035.
75. Mi Li, Xiubin Xiao, Lianqing Liu, Ning Xi, Yuechao Wang, Zaili Dong, and Weijing Zhang. Nanoscale mapping and organization analysis of target proteins on cancer cells from B-cell lymphoma patients. *Experimental Cell Research*, 319(18):2812–2821, 2013. ISSN 00144827. doi: 10.1016/j.yexcr.2013.07.020.
76. Manfred B Lutz, Nicole Kukutsch, Alexandra L.J Ogilvie, Susanne Rößner, Franz Koch, Nikolaus Romani, and Gerold Schuler. An advanced culture method for generating large quantities of highly pure dendritic cells from mouse bone marrow. *Journal of Immunological Methods*, 223(1):77–92, 1999. ISSN 00221759. doi: 10.1016/S0022-1759(98)00204-X.

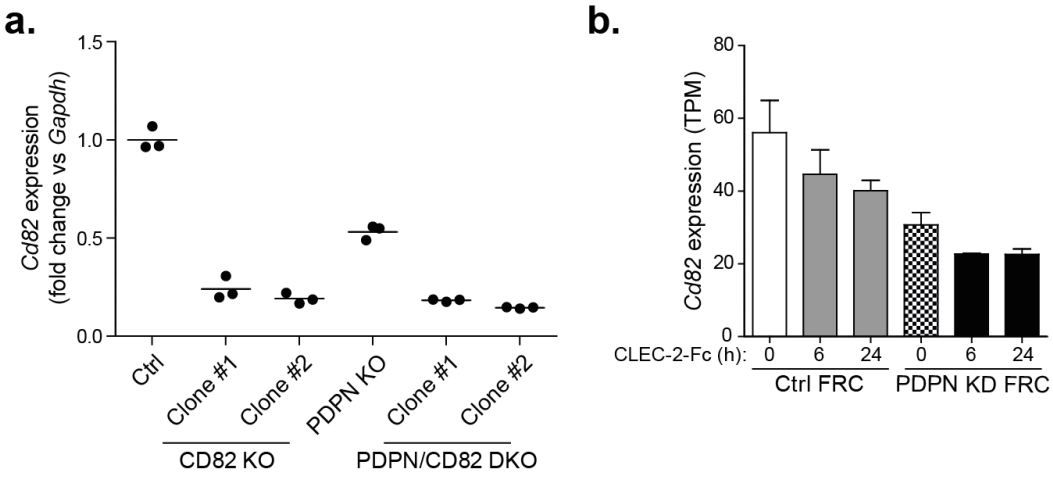

Fig. S1. CD82 expression in FRC cell lines. a. Two single clones of CD82 knock-out (KO) and PDPN/CD82 double-KO (DKO) FRCs were validated using *Cd82* mRNA expression by lack of a good CD82 antibody for flow cytometry. *Cd82* mRNA expression is calculated as fold change of *Gapdh* expression. n=3 technical replicates for each cell line, and representative data from n=2 biological replicates is shown. **b.** *Cd82* mRNA expression in control (Ctrl) and podoplanin siRNA knock-down (PDPN KD) FRC cell lines as measured by RNA sequencing. FRCs were treated for 6 or 24 hours with CLEC-2-Fc. n=4 biological replicates. Data shown as mean+SD. TPM, transcripts per million.

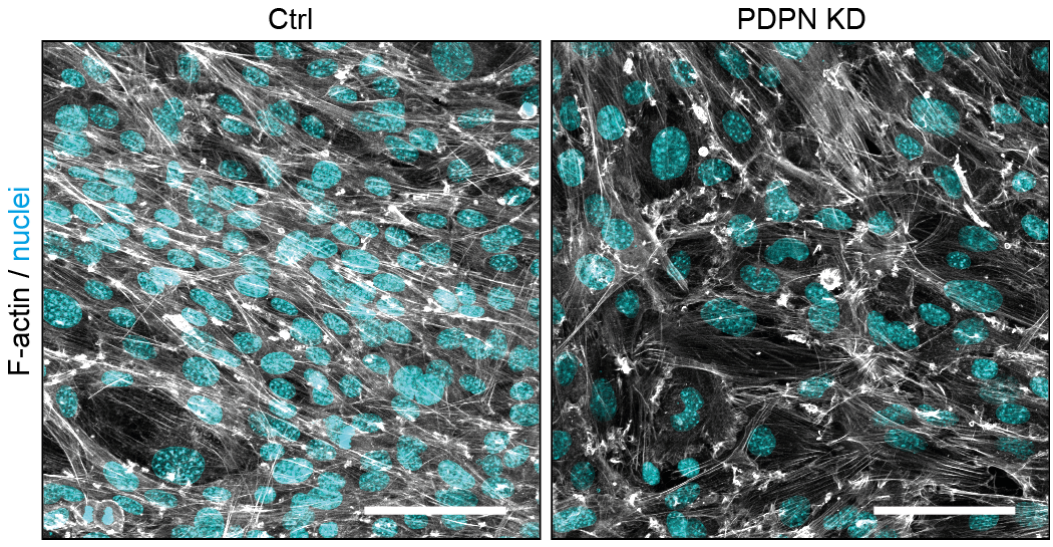

Fig. S2. FRC-FRC interaction is podoplanin-dependent. Ctrl (left) and PDPN KD (right) FRCs were cultured until full confluency was reached. Ctrl FRCs align with each other in one direction, unlike PDPN KD FRCs. FRCs were stained for F-actin (grey) and cell nuclei (cyan). The scale bars represent 100 microns.

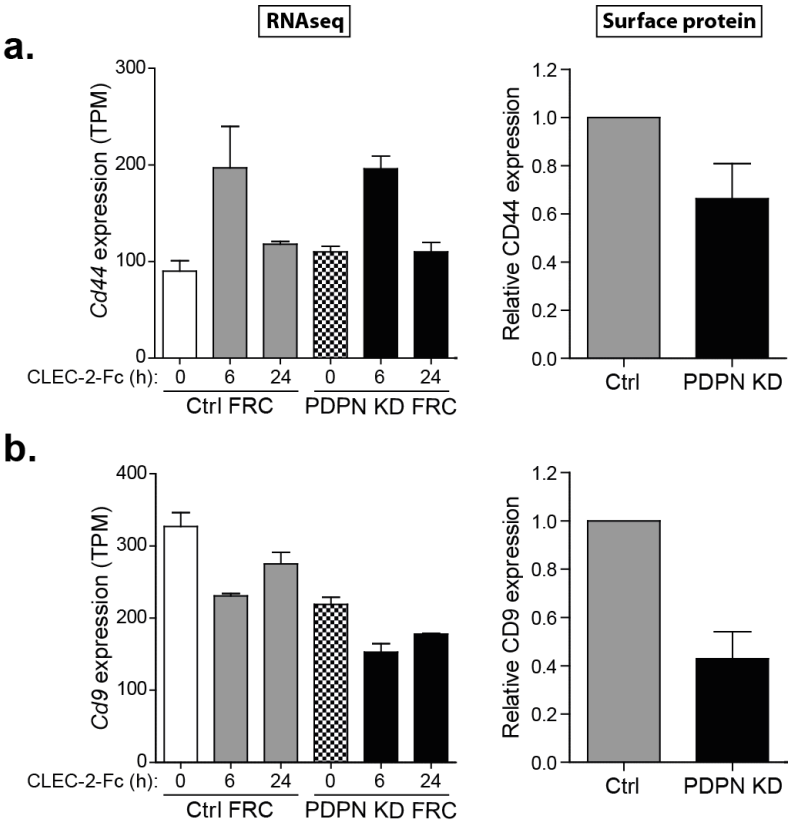

Fig. S3. CD44 and CD9 expression correlates with podoplanin expression. CD44 (**a**) and CD9 (**b**) mRNA (left; RNA sequencing) and surface protein (right; flow cytometry) expression in control (Ctrl) and podoplanin siRNA knock-down (PDPN KD) FRC cell lines. For RNAseq, FRCs were treated for 6 or 24 hours with CLEC-2-Fc. n=4 biological replicates. Data shown as mean+SD. TPM, transcripts per million.

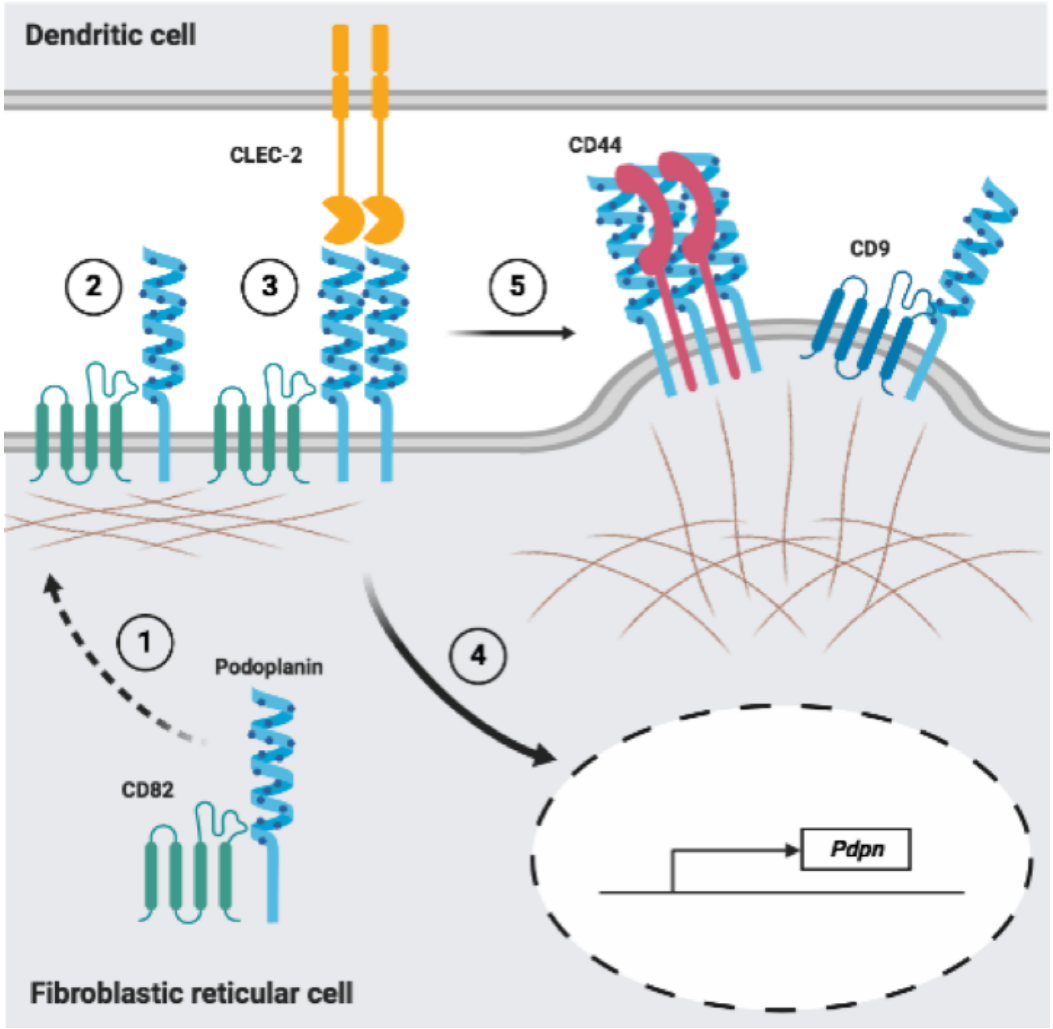

Fig. S4. Model representing the different functions of podoplanin on fibroblastic reticular cells mediated by changing interactions with its partner proteins. **1)** Tetraspanin CD82 is required for podoplanin expression on the cell surface, most likely via a trafficking mechanism. We hypothesize that podoplanin remains with CD82 in the same protein complex to maintain podoplanin expression at the cell surface. **2)** In homeostasis, podoplanin links to the actin cytoskeleton via ERM proteins, which drives actomyosin contractility (Acton2014, Astarita2015). **3)** Upon initiation of an immune response, CLEC-2^{hi} dendritic cells arrive in the lymph node, and migrate along the FRC network by interacting with podoplanin, which results in protein clustering (Acton2014). **4)** CLEC-2 binding to podoplanin drives a transcriptional response (Martinez2019), resulting in increased podoplanin expression. **5)** CLEC-2 binding switches podoplanin function from actomyosin contractility to FRC spreading. This is controlled by podoplanin binding proteins CD44 and CD9, which drives formation of lamellipodia-like and filopodia-like protrusions, respectively. Furthermore, CD9 is involved establishing FRC-FRC interactions, thereby potentially playing an important role in formation of the FRC network (not depicted). Image created with BioRender.com

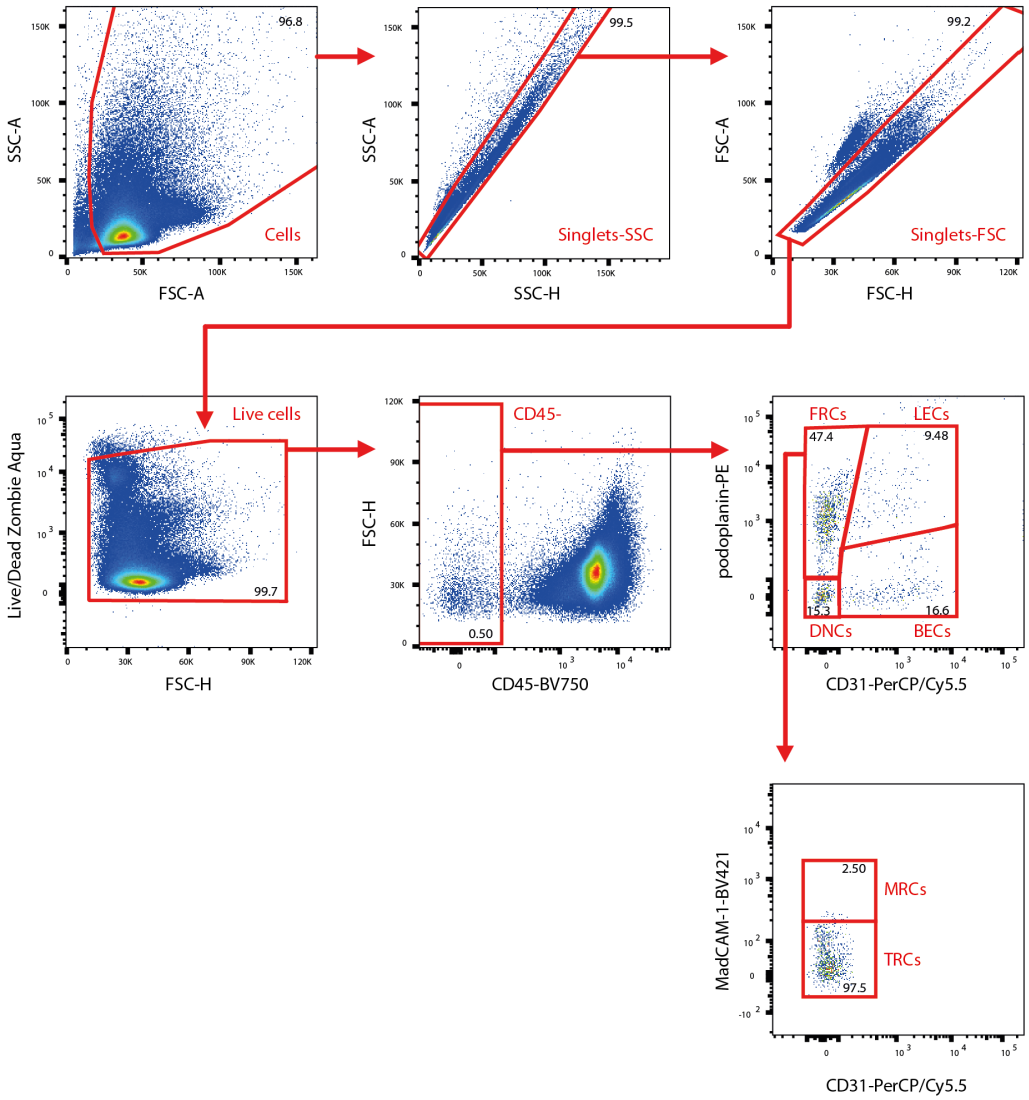

Fig. S5. Gating strategy for analysis of *in vivo* immunised lymph nodes. All gates are based on FMOs (fluorescence minus one samples) and relevant controls. Numbers indicated percentage of parental population. BECs = blood endothelial cells, BV = Brilliant Violet, DNCs = double negative cells, FRCs = fibroblastic reticular cells, LECs = lymphatic endothelial cells, MRCs = marginal reticular cells, TRCs = T-zone fibroblastic reticular cells.